The Astrophysical Journal, 783:130 (14pp), 2014 March 10 doi:10.1088/0004-637X/783/2/130

TRIGONOMETRIC PARALLAXES OF HIGH MASS STAR FORMING REGIONS: THE STRUCTURE AND KINEMATICS OF THE MILKY WAY

M. J. Reid[1], K. M. Menten[2], A. Brunthaler[2], X. W. Zheng[3], T. M. Dame[1], Y. Xu[4], Y. Wu[2], B. Zhang[2], A. Sanna[2], M. Sato[2], K. Hachisuka[5], Y. K. Choi[2], K. Immer[2], L. Moscadelli[6], K. L. J. Rygl[7], and A. Bartkiewicz[8]
[1] Harvard-Smithsonian Center for Astrophysics, 60 Garden Street, Cambridge, MA 02138, USA
[2] Max-Planck-Institut für Radioastronomie, Auf dem Hügel 69, D-53121 Bonn, Germany
[3] Department of Astronomy, Nanjing University Nanjing 210093, China
[4] Purple Mountain Observatory, Chinese Academy of Sciences, Nanjing 210008, China
[5] Shanghai Astronomical Observatory, 80 Nandan Rd., Shanghai, China
[6] Arcetri Observatory, Firenze, Italy
[7] European Space Agency (ESA-ESTEC), Keplerlaan 1, P.O. Box 299, 2200 AG, Noordwijk, The Netherlands
[8] Centre for Astronomy, Faculty of Physics, Astronomy and Informatics, Nicolaus Copernicus University, Grudziadzka 5, 87-100 Torun, Poland
Received 2013 November 5; accepted 2014 January 13; published 2014 February 24

ABSTRACT

Over 100 trigonometric parallaxes and proper motions for masers associated with young, high-mass stars have been measured with the Bar and Spiral Structure Legacy Survey, a Very Long Baseline Array key science project, the European VLBI Network, and the Japanese VLBI Exploration of Radio Astrometry project. These measurements provide strong evidence for the existence of spiral arms in the Milky Way, accurately locating many arm segments and yielding spiral pitch angles ranging from about 7° to 20°. The widths of spiral arms increase with distance from the Galactic center. Fitting axially symmetric models of the Milky Way with the three-dimensional position and velocity information and conservative priors for the solar and average source peculiar motions, we estimate the distance to the Galactic center, R_0, to be 8.34 ± 0.16 kpc, a circular rotation speed at the Sun, Θ_0, to be 240 ± 8 km s^{-1}, and a rotation curve that is nearly flat (i.e., a slope of -0.2 ± 0.4 km s^{-1} kpc^{-1}) between Galactocentric radii of ≈5 and 16 kpc. Assuming a "universal" spiral galaxy form for the rotation curve, we estimate the thin disk scale length to be 2.44 ± 0.16 kpc. With this large data set, the parameters R_0 and Θ_0 are no longer highly correlated and are relatively insensitive to different forms of the rotation curve. If one adopts a theoretically motivated prior that high-mass star forming regions are in nearly circular Galactic orbits, we estimate a global solar motion component in the direction of Galactic rotation, $V_\odot = 14.6 \pm 5.0$ km s^{-1}. While Θ_0 and $V_\odot$ are significantly correlated, the sum of these parameters is well constrained, $\Theta_0 + V_\odot = 255.2 \pm 5.1$ km s^{-1}, as is the angular speed of the Sun in its orbit about the Galactic center, $(\Theta_0 + V_\odot)/R_0 = 30.57 \pm 0.43$ km s^{-1} kpc^{-1}. These parameters improve the accuracy of estimates of the accelerations of the Sun and the Hulse–Taylor binary pulsar in their Galactic orbits, significantly reducing the uncertainty in tests of gravitational radiation predicted by general relativity.

Key words: Galaxy: fundamental parameters – Galaxy: kinematics and dynamics – Galaxy: structure – gravitational waves – parallaxes – stars: formation

Online-only material: color figures, machine readable table

1. INTRODUCTION

Two major projects to map the spiral structure of the Milky Way are providing parallaxes and proper motions for water and methanol masers associated with high-mass star forming regions (HMSFRs) across large portions of the Milky Way. The Bar and Spiral Structure Legacy (BeSSeL) Survey[9] and the Japanese VLBI Exploration of Radio Astrometry (VERA)[10] have yielded over 100 parallax measurements with accuracies typically about ±20 μas, and some as good as ±5 μas. This accuracy exceeds the target of the European astrometric satellite mission Gaia, launched in 2013 December and scheduled for final results in 2021–2022 (Eyer et al. 2013). While Gaia aims to measure ∼10^9 stars, far more than practical by very long baseline interferometry (VLBI), Gaia will be limited by extinction at optical wavelengths and will not be able to freely probe the Galactic plane. In contrast, VLBI at radio wavelengths is not affected by dust extinction and can yield parallaxes for massive young stars that best trace spiral structure in other galaxies, and current parallax accuracy allows measurements for stars across most of the Milky Way.

Given parallax and proper motion measurements (coupled with source coordinates and line-of-sight velocities from Doppler shifts of spectral lines), one has complete phase-space information. This provides direct and powerful constraints on the fundamental parameters of the Galaxy, including the distance to the Galactic center, R_0, and the circular orbital speed at the Sun, Θ_0. Preliminary models of the structure and dynamics of the Galaxy based on VLBI parallax and proper motions of star forming regions have been published. Reid et al. (2009b) fitted results from 16 HMSFRs and determined $R_0 = 8.4 \pm 0.6$ kpc and $\Theta_0 = 254 \pm 16$ km s^{-1}, assuming the solar motion in the direction of Galactic rotation, $V_\odot$, is 5 km s^{-1} (Dehnen & Binney 1998). More recently Honma et al. (2012) analyzed results from a larger sample of 52 sources, including both low-mass star forming regions and HMSFRs, and concluded that $R_0 = 8.05 \pm 0.45$ kpc and $\Theta_0 = 238 \pm 14$ km s^{-1}, assuming $V_\odot = 12$ km s^{-1} (Schoenrich et al. 2010). Several groups have re-modeled maser parallax and proper motion data (Bovy et al.

[9] http://bessel.vlbi-astrometry.org
[10] http://veraserver.mtk.nao.ac.jp

2009; McMillan & Binney 2010; Bobylev & Bajkova 2010) using different approaches and focusing on effects of parameter correlations and prior assumptions, most notably the values adopted for the solar motion (see Sections 4.2 and 5.1).

With the much larger number and wider distribution of parallaxes and proper motions of HMSFRs now available, we can provide more robust estimates of the fundamental Galactic parameters. In Section 2, we present the combined parallax data sets from the BeSSeL and VERA groups and comment on aspects of spiral structure in Section 3. We model the combined data set to obtain better estimates of R_0 and Θ_0 in Section 4, including discussion of priors, different forms of rotation curves, and parameter correlations. Finally, in Section 5, we discuss the solar motion, best values for R_0 and Θ_0, and some astrophysical implications.

2. PARALLAXES AND PROPER MOTIONS

Table 1 lists the parallaxes and proper motions of 103 regions of high-mass star formation measured with VLBI techniques, using the National Radio Astronomy Observatory's Very Long Baseline Array (VLBA), the Japanese VERA project, and the European VLBI Network (EVN). We have include three red supergiants (NML Cyg, S Per, VY CMa) as indicative of HMSFRs, since they are high mass stars that have short lifetimes ($<10^7$ yr) and therefore cannot have migrated far from their birth locations. The locations of these star forming regions in the Galaxy are shown in Figure 1, superposed on a schematic diagram of the Milky Way. Distance errors are indicated with error bars (1σ), but for many sources the error bars are smaller than the symbols.

Both the proper motion, μ_x and μ_y, and local standard of rest (LSR) velocity, $v_{\rm LSR}$, values and their uncertainties are meant to apply to the central star (or stars) that excite the masers. (Note that "LSR velocities" are *defined* based on the standard solar motion values of 20 km s^{-1} toward 18^h right ascension and 30° declination in 1900 coordinates, which translate to Galactic Cartesian components of $U_\odot^{\rm Std} = 10$, $V_\odot^{\rm Std} = 15$ and $W_\odot^{\rm Std} = 7$ km s^{-1}.) For the $v_{\rm LSR}$ values we adopted methanol maser values, when available, or CO emission values from associated giant molecular clouds. Since some of the references reporting parallax and proper motion present only measurement uncertainty, for these we estimated an additional error term associated with the uncertainty in transferring the maser motions to that of the central star. These were added in quadrature with the measurement uncertainties. For methanol masers, which typically have modest motions of $\lesssim$10 km s^{-1} with respect to the central star, we estimated the additional error term to be ±5 km s^{-1} for $v_{\rm LSR}$ and a corresponding value for the proper motion components at the measured distance. While some water masers have expansion motions comparable to methanol masers, others display much faster outflow motions. High velocity outflows are usually associated with water masers that have spectra rich in features, spread over many tens of km s^{-1}. We, therefore, evaluated the richness and spread of the water spectra (with respect to the systemic velocity as indicated by CO emission) and assigned the additional error term for μ_x and μ_y values between 5 and 20 km s^{-1}.

3. SPIRAL STRUCTURE

Spiral arms in the Milky Way have long been recognized as presenting coherent arcs and loops in Galactic longitude–velocity (ℓ–V) plots of atomic and molecular emissions. However, transforming velocity to distance (i.e., kinematic distances) has been problematic, owing to near-far distance ambiguities in the first and fourth Galactic quadrants and significant distance errors owing to large peculiar motions for some arm material (see, e.g., Xu et al. 2006; Reid et al. 2009b). While one cannot accurately place spiral arms on a plan view of the Milky Way from ℓ–V plots, one can in most cases unambiguously assign HMSFRs to spiral arms by association with CO and H I emission features. We have done this for the vast majority of the HMSFRs for which parallax and proper motions have been measured (Hachisuka et al. 2014; Choi et al. 2014; Zhang et al. 2013; Xu et al. 2013; Wu et al. 2014; Sato et al. 2014; Sanna et al. 2014), as indicated in Table 1 and Figure 1. This avoids using the measured distances (parallaxes) and subjective judgment based on spatial location for arm assignments.

There are two avenues for checking that the arm assignments are reliable. Firstly, and most straightforwardly, looking at a plan view of the Milky Way (see Figure 1) on which star forming regions with parallax distances are located, one can see that the pattern of sources for any given arm traces a continuous arc that resembles a spiral arm in external galaxies. Also, there are clear inter-arm regions with few, if any, HMSFRs between the Outer, Perseus, Local, Sagittarius, and Scutum arms. However, as one looks to the inner Galaxy, the current parallax data are not adequate to clearly separate arms, presuming significant separations even exist.

Secondly, once sources are assigned to arms based on ℓ–V information, one can then attempt to fit their radial and azimuthal locations to log-periodic spiral forms using measured distances. In the papers cited above, we fitted spiral patterns to arm segments, adopting a log-periodic spiral defined by

$$\ln(R/R_{\rm ref}) = -(\beta - \beta_{\rm ref})\tan\psi,$$

where R is the Galactocentric radius at a Galactocentric azimuth β (defined as 0 toward the Sun and increasing with Galactic longitude) for an arm with a radius $R_{\rm ref}$ at reference azimuth $\beta_{\rm ref}$ and pitch angle ψ. We fitted a straight line to (x, y)=$(\beta, \ln(R/R_{\rm ref}))$ using a Bayesian Markov chain Monte Carlo (McMC) procedure to estimate the parameters $R_{\rm ref}$ and ψ. (The reference azimuth, $\beta_{\rm ref}$, was arbitrarily set near the midpoint of the azimuth values for the sources in an arm). We minimized the "distance" perpendicular to the fitted straight line by rotating (x, y) through the angle ψ to (x_r, y_r), i.e.,

$$x_r = x\cos\psi + y\sin\psi;\; y_r = y\cos\psi - x\sin\psi,$$

such that the best-fitting line lay in the x_r axis.

Uncertainties in the source parallax "map" into both coordinates and were estimated numerically by randomly drawing trial parallax values (consistent with the measured values and uncertainties) and calculating the root-mean-squares for trial $\ln(R/R_{\rm ref})$ and β values. The locations of the HMSFRs deviated from fitted spirals by more than could be explained by parallax uncertainties. This is expected for spiral arms with intrinsic widths of several hundred parsecs. In order to allow for (and estimate) the scatter in location expected from the width of the spiral arm, before calculating trial $\ln(R/R_{\rm ref})$ values, we added random scatter to the trial R values via $R \leftarrow R + g a_w \cos\psi$, where g is a random number drawn from a Gaussian distribution with zero mean and unity standard deviation and a_w is an arm-width parameter, adjusted to give a post-fit χ^2_ν near unity. The uncertainties in $(\beta, \ln(R/R_{\rm ref}))$ were then rotated by angle ψ to match the data.

Table 1
Parallaxes and Proper Motions of High-mass Star Forming Regions

Source	Alias	R.A. (hh:mm:ss)	Decl. (dd:mm:ss)	Parallax (mas)	μ_x (mas yr^{-1})	μ_y (mas yr^{-1})	$v_{\rm LSR}$ (km s^{-1})	Spiral Arm	Refs.
G348.70−01.04		17:20:04.04	−38:58:30.9	0.296 ± 0.026	−0.73 ± 0.19	−2.83 ± 0.54	−7 ± 6	...	1
G351.44+00.65	NGC 6334	17:20:54.60	−35:45:08.6	0.744 ± 0.074	0.40 ± 0.51	−2.24 ± 0.64	−8 ± 3	Sgr	2
G000.67−00.03	Sgr B2	17:47:20.00	−28:22:40.0	0.129 ± 0.012	−0.78 ± 0.40	−4.26 ± 0.40	62 ± 5	...	3
G005.88−00.39		18:00:30.31	−24:04:04.5	0.334 ± 0.020	0.18 ± 0.34	−2.26 ± 0.34	9 ± 3	Sct	4
G009.62+00.19		18:06:14.66	−20:31:31.7	0.194 ± 0.023	−0.58 ± 0.13	−2.49 ± 0.29	2 ± 3	4−k	5
G010.47+00.02		18:08:38.23	−19:51:50.3	0.117 ± 0.008	−3.86 ± 0.19	−6.40 ± 0.14	69 ± 5	Con	7
G010.62−00.38	W 31	18:10:28.55	−19:55:48.6	0.202 ± 0.019	−0.37 ± 0.50	−0.60 ± 0.25	−3 ± 5	3−k	7
G011.49−01.48		18:16:22.13	−19:41:27.2	0.800 ± 0.033	1.42 ± 0.52	−0.60 ± 0.65	11 ± 3	Sgr	2
G011.91−00.61		18:13:58.12	−18:54:20.3	0.297 ± 0.031	0.66 ± 0.28	−1.36 ± 0.41	37 ± 5	Sct	4
G012.02−00.03		18:12:01.84	−18:31:55.8	0.106 ± 0.008	−4.11 ± 0.07	−7.76 ± 0.27	108 ± 5	3−k	7
G012.68−00.18		18:13:54.75	−18:01:46.6	0.416 ± 0.028	−1.00 ± 0.95	−2.85 ± 0.95	58 ± 10	Sct	8
G012.80−00.20		18:14:14.23	−17:55:40.5	0.343 ± 0.037	−0.60 ± 0.70	−0.99 ± 0.70	34 ± 5	Sct	8
G012.88+00.48	IRAS 18089−1732	18:11:51.42	−17:31:29.0	0.400 ± 0.040	0.15 ± 0.25	−2.30 ± 0.39	31 ± 7	Sct	8, 10
G012.90−00.24		18:14:34.42	−17:51:51.9	0.408 ± 0.025	0.19 ± 0.80	−2.52 ± 0.80	36 ± 10	Sct	8
G012.90−00.26		18:14:39.57	−17:52:00.4	0.396 ± 0.032	−0.36 ± 0.80	−2.22 ± 0.80	39 ± 10	Sct	8
G013.87+00.28		18:14:35.83	−16:45:35.9	0.254 ± 0.024	−0.25 ± 2.00	−2.49 ± 2.00	48 ± 10	Sct	4
G014.33−00.64		18:18:54.67	−16:47:50.3	0.893 ± 0.101	0.95 ± 1.50	−2.40 ± 1.30	22 ± 5	Sgr	9
G014.63−00.57		18:19:15.54	−16:29:45.8	0.546 ± 0.022	0.22 ± 1.20	−2.07 ± 1.20	19 ± 5	Sgr	2
G015.03−00.67	M 17	18:20:24.81	−16:11:35.3	0.505 ± 0.033	0.68 ± 0.32	−1.42 ± 0.33	22 ± 3	Sgr	10
G016.58−00.05		18:21:09.08	−14:31:48.8	0.279 ± 0.023	−2.52 ± 0.37	−2.33 ± 0.35	60 ± 5	Sct	4
G023.00−00.41		18:34:40.20	−09:00:37.0	0.218 ± 0.017	−1.72 ± 0.14	−4.12 ± 0.33	80 ± 3	4−k	11
G023.44−00.18		18:34:39.19	−08:31:25.4	0.170 ± 0.032	−1.93 ± 0.15	−4.11 ± 0.13	97 ± 3	4−k	11
G023.65−00.12		18:34:51.59	−08:18:21.4	0.313 ± 0.039	−1.32 ± 0.20	−2.96 ± 0.20	83 ± 3	...	12
G023.70−00.19		18:35:12.36	−08:17:39.5	0.161 ± 0.024	−3.17 ± 0.12	−6.38 ± 0.16	73 ± 5	4−k	7
G025.70+00.04		18:38:03.14	−06:24:15.5	0.098 ± 0.029	−2.89 ± 0.07	−6.20 ± 0.36	93 ± 5	Sct	4
G027.36−00.16		18:41:51.06	−05:01:43.4	0.125 ± 0.042	−1.81 ± 0.11	−4.11 ± 0.27	92 ± 3	Sct	10
G028.86+00.06		18:43:46.22	−03:35:29.6	0.135 ± 0.018	−4.80 ± 0.30	−5.90 ± 0.30	100 ± 10	Sct	4
G029.86−00.04		18:45:59.57	−02:45:06.7	0.161 ± 0.020	−2.32 ± 0.11	−5.29 ± 0.16	100 ± 3	Sct	6
G029.95−00.01	W 43S	18:46:03.74	−02:39:22.3	0.190 ± 0.019	−2.30 ± 0.13	−5.34 ± 0.13	98 ± 3	Sct	6
G031.28+00.06		18:48:12.39	−01:26:30.7	0.234 ± 0.039	−2.09 ± 0.16	−4.37 ± 0.21	109 ± 3	Sct	6
G031.58+00.07	W 43Main	18:48:41.68	−01:09:59.0	0.204 ± 0.030	−1.88 ± 0.40	−4.84 ± 0.40	96 ± 5	Sct	6
G032.04+00.05		18:49:36.58	−00:45:46.9	0.193 ± 0.008	−2.21 ± 0.40	−4.80 ± 0.40	97 ± 5	Sct	4
G033.64−00.22		18:53:32.56	+00:31:39.1	0.153 ± 0.017	−3.18 ± 0.10	−6.10 ± 0.10	60 ± 3	...	1
G034.39+00.22		18:53:18.77	+01:24:08.8	0.643 ± 0.049	−0.90 ± 1.00	−2.75 ± 2.00	57 ± 5	Sgr	13
G035.02+00.34		18:54:00.67	+02:01:19.2	0.430 ± 0.040	−0.92 ± 0.90	−3.61 ± 0.90	52 ± 5	Sgr	2
G035.19−00.74		18:58:13.05	+01:40:35.7	0.456 ± 0.045	−0.18 ± 0.50	−3.63 ± 0.50	30 ± 7	Sgr	14
G035.20−01.73		19:01:45.54	+01:13:32.5	0.306 ± 0.045	−0.71 ± 0.21	−3.61 ± 0.26	42 ± 3	Sgr	14
G037.43+01.51		18:54:14.35	+04:41:41.7	0.532 ± 0.021	−0.45 ± 0.35	−3.69 ± 0.39	41 ± 3	Sgr	2
G043.16+00.01	W 49N	19:10:13.41	+09:06:12.8	0.090 ± 0.007	−2.88 ± 0.20	−5.41 ± 0.20	10 ± 5	Per	15
G043.79−00.12	OH 43.8−0.1	19:11:53.99	+09:35:50.3	0.166 ± 0.005	−3.02 ± 0.36	−6.20 ± 0.36	44 ± 10	Sgr	2
G043.89−00.78		19:14:26.39	+09:22:36.5	0.121 ± 0.020	−2.75 ± 0.30	−6.43 ± 0.30	54 ± 5	Sgr	2
G045.07+00.13		19:13:22.04	+10:50:53.3	0.125 ± 0.005	−2.98 ± 0.45	−6.26 ± 0.45	59 ± 5	Sgr	2
G045.45+00.05		19:14:21.27	+11:09:15.9	0.119 ± 0.017	−2.34 ± 0.38	−6.00 ± 0.54	55 ± 7	Sgr	2
G048.60+00.02		19:20:31.18	+13:55:25.2	0.093 ± 0.005	−2.89 ± 0.13	−5.50 ± 0.13	18 ± 5	Per	15
G049.19−00.33		19:22:57.77	+14:16:10.0	0.189 ± 0.007	−2.99 ± 0.40	−5.71 ± 0.40	67 ± 5	Sgr	2
G049.48−00.36	W 51 IRS2	19:23:39.82	+14:31:05.0	0.195 ± 0.071	−2.49 ± 0.14	−5.51 ± 0.16	56 ± 3	Sgr	16
G049.48−00.38	W 51M	19:23:43.87	+14:30:29.5	0.185 ± 0.010	−2.64 ± 0.20	−5.11 ± 0.20	58 ± 4	Sgr	17
G052.10+01.04	IRAS 19213+1723	19:23:37.32	+17:29:10.5	0.251 ± 0.060	−2.60 ± 2.00	−6.10 ± 2.00	42 ± 5	Sgr	18
G059.78+00.06		19:43:11.25	+23:44:03.3	0.463 ± 0.020	−1.65 ± 0.30	−5.12 ± 0.30	25 ± 3	Loc	16
G069.54−00.97	ON 1	20:10:09.07	+31:31:36.0	0.406 ± 0.013	−3.19 ± 0.40	−5.22 ± 0.40	12 ± 5	Loc	19, 20, 21
G074.03−01.71		20:25:07.11	+34:49:57.6	0.629 ± 0.017	−3.79 ± 1.30	−4.88 ± 1.50	5 ± 5	Loc	21
G075.29+01.32		20:16:16.01	+37:35:45.8	0.108 ± 0.005	−2.37 ± 0.11	−4.48 ± 0.17	−58 ± 5	Out	22
G075.76+00.33		20:21:41.09	+37:25:29.3	0.285 ± 0.022	−3.08 ± 0.60	−4.56 ± 0.60	−9 ± 9	Loc	21
G075.78+00.34	ON 2N	20:21:44.01	+37:26:37.5	0.261 ± 0.030	−2.79 ± 0.55	−4.66 ± 0.55	1 ± 5	Loc	23
G076.38−00.61		20:27:25.48	+37:22:48.5	0.770 ± 0.053	−3.73 ± 3.00	−3.84 ± 3.00	−2 ± 5	Loc	21
G078.12+03.63	IRAS 20126+4104	20:14:26.07	+41:13:32.7	0.610 ± 0.030	−2.06 ± 0.50	0.98 ± 0.50	−4 ± 5	Loc	24
G078.88+00.70	AFGL 2591	20:29:24.82	+40:11:19.6	0.300 ± 0.024	−1.20 ± 0.72	−4.80 ± 0.66	−6 ± 7	Loc	25
G079.73+00.99	IRAS 20290+4052	20:30:50.67	+41:02:27.5	0.737 ± 0.062	−2.84 ± 0.50	−4.14 ± 0.70	−3 ± 5	Loc	25
G079.87+01.17		20:30:29.14	+41:15:53.6	0.620 ± 0.027	−3.23 ± 1.30	−5.19 ± 1.30	−5 ± 10	Loc	21
G080.79−01.92	NML Cyg	20:46:25.54	+40:06:59.4	0.620 ± 0.047	−1.55 ± 0.57	−4.59 ± 0.57	−3 ± 3	Loc	26
G080.86+00.38	DR 20	20:37:00.96	+41:34:55.7	0.687 ± 0.038	−3.29 ± 0.45	−4.83 ± 0.50	−3 ± 5	Loc	25
G081.75+00.59	DR 21	20:39:01.99	+42:24:59.3	0.666 ± 0.035	−2.84 ± 0.45	−3.80 ± 0.47	−3 ± 3	Loc	25
G081.87+00.78	W 75N	20:38:36.43	+42:37:34.8	0.772 ± 0.042	−1.97 ± 0.50	−4.16 ± 0.51	7 ± 3	Loc	25
G090.21+02.32		21:02:22.70	+50:03:08.3	1.483 ± 0.038	−0.67 ± 1.56	−0.90 ± 1.67	−3 ± 5	Loc	21
G092.67+03.07		21:09:21.73	+52:22:37.1	0.613 ± 0.020	−0.69 ± 0.60	−2.25 ± 0.60	−5 ± 10	Loc	21

Table 1
(Continued)

Source	Alias	R.A. (hh:mm:ss)	Decl. (dd:mm:ss)	Parallax (mas)	μ_x (mas yr^{-1})	μ_y (mas yr^{-1})	v_{LSR} (km s^{-1})	Spiral Arm	Refs.
G094.60−01.79	AFGL 2789	21:39:58.27	+50:14:21.0	0.280 ± 0.030	−2.30 ± 0.60	−3.80 ± 0.60	−46 ± 5	Per	18, 28
G095.29−00.93		21:39:40.51	+51:20:32.8	0.205 ± 0.015	−2.75 ± 0.20	−2.75 ± 0.25	−38 ± 5	Per	28
G097.53+03.18		21:32:12.43	+55:53:49.7	0.133 ± 0.017	−2.94 ± 0.29	−2.48 ± 0.29	−73 ± 5	Out	27
G100.37−03.57		22:16:10.37	+52:21:34.1	0.291 ± 0.010	−3.77 ± 0.60	−3.12 ± 0.60	−37 ± 10	Per	28
G105.41+09.87		21:43:06.48	+66:06:55.3	1.129 ± 0.063	−0.21 ± 1.20	−5.49 ± 1.20	−10 ± 5	Loc	21
G107.29+05.63	IRAS 22198+6336	22:21:26.73	+63:51:37.9	1.288 ± 0.107	−2.47 ± 1.40	0.26 ± 1.40	−11 ± 5	Loc	29
G108.18+05.51	L 1206	22:28:51.41	+64:13:41.3	1.289 ± 0.153	0.27 ± 0.50	−1.40 ± 1.95	−11 ± 3	Loc	19
G108.20+00.58		22:49:31.48	+59:55:42.0	0.229 ± 0.028	−2.25 ± 0.50	−1.00 ± 0.50	−49 ± 5	Per	28
G108.47−02.81		23:02:32.08	+56:57:51.4	0.309 ± 0.010	−2.45 ± 1.00	−3.00 ± 0.70	−54 ± 5	Per	28
G108.59+00.49		22:52:38.30	+60:00:52.0	0.398 ± 0.031	−5.55 ± 0.40	−3.38 ± 0.40	−52 ± 5	Per	28
G109.87+02.11	Cep A	22:56:18.10	+62:01:49.5	1.430 ± 0.080	0.50 ± 1.50	−3.70 ± 1.00	−7 ± 5	Loc	30
G111.23−01.23		23:17:20.79	+59:28:47.0	0.288 ± 0.044	−4.28 ± 0.60	−2.33 ± 0.60	−53 ± 10	Per	28
G111.25−00.76		23:16:10.36	+59:55:28.5	0.294 ± 0.016	−2.45 ± 0.60	−2.10 ± 0.60	−43 ± 5	Per	28
G111.54+00.77	NGC 7538	23:13:45.36	+61:28:10.6	0.378 ± 0.017	−2.45 ± 0.24	−2.44 ± 0.25	−57 ± 5	Per	30
G121.29+00.65	L 1287	00:36:47.35	+63:29:02.2	1.077 ± 0.039	−0.86 ± 0.76	−2.29 ± 0.82	−23 ± 5	Loc	19
G122.01−07.08	IRAS 00420+5530	00:44:58.40	+55:46:47.6	0.460 ± 0.020	−3.70 ± 0.50	−1.25 ± 0.50	−50 ± 5	Per	31
G123.06−06.30	NGC 281	00:52:24.70	+56:33:50.5	0.355 ± 0.030	−2.79 ± 0.62	−2.14 ± 0.70	−30 ± 5	Per	32
G123.06−06.30	NGC 281W	00:52:24.20	+56:33:43.2	0.421 ± 0.022	−2.69 ± 0.31	−1.77 ± 0.29	−29 ± 3	Per	19
G133.94+01.06	W 3OH	02:27:03.82	+61:52:25.2	0.512 ± 0.010	−1.20 ± 0.32	−0.15 ± 0.32	−47 ± 3	Per	33, 34
G134.62−02.19	S Per	02:22:51.71	+58:35:11.4	0.413 ± 0.017	−0.49 ± 0.35	−1.19 ± 0.33	−39 ± 5	Per	35
G135.27+02.79	WB 89−437	02:43:28.57	+62:57:08.4	0.167 ± 0.011	−1.22 ± 0.30	0.46 ± 0.36	−72 ± 3	Out	36
G160.14+03.15		05:01:40.24	+47:07:19.0	0.244 ± 0.006	0.87 ± 0.35	−1.32 ± 0.29	−18 ± 5	...	1
G168.06+00.82	IRAS 05137+3919	05:17:13.74	+39:22:19.9	0.130 ± 0.040	0.50 ± 0.24	−0.85 ± 0.17	−27 ± 5	Out	37, 38
G176.51+00.20		05:37:52.14	+32:00:03.9	1.038 ± 0.021	1.84 ± 1.00	−5.86 ± 1.00	−17 ± 5	Loc	21
G182.67−03.26		05:39:28.42	+24:56:32.1	0.149 ± 0.011	0.16 ± 0.32	−0.17 ± 0.32	−7 ± 10	Out	37
G183.72−03.66		05:40:24.23	+23:50:54.7	0.570 ± 0.013	0.13 ± 1.20	−1.40 ± 1.20	3 ± 5	Per	28
G188.79+01.03	IRAS 06061+2151	06:09:06.97	+21:50:41.4	0.496 ± 0.103	−0.10 ± 0.50	−3.91 ± 0.50	−5 ± 5	Per	39
G188.94+00.88	S 252	06:08:53.35	+21:38:28.7	0.476 ± 0.006	0.02 ± 0.30	−2.02 ± 0.30	8 ± 5	Per	18, 40
G192.16−03.81		05:58:13.53	+16:31:58.9	0.660 ± 0.040	0.70 ± 0.78	−1.80 ± 0.86	5 ± 5	Per	41
G192.60−00.04	S 255	06:12:54.02	+17:59:23.3	0.628 ± 0.027	−0.14 ± 0.67	−0.84 ± 1.80	6 ± 5	Per	19
G196.45−01.67	S 269	06:14:37.08	+13:49:36.7	0.189 ± 0.012	−0.42 ± 0.20	−0.12 ± 0.20	19 ± 5	Out	42
G209.00−19.38	Orion Nebula	05:35:15.80	−05:23:14.1	2.410 ± 0.030	3.30 ± 1.50	0.10 ± 1.50	3 ± 5	Loc	43, 44, 45
G211.59+01.05		06:52:45.32	+01:40:23.1	0.228 ± 0.007	−0.93 ± 0.24	0.71 ± 0.26	45 ± 5	...	1
G229.57+00.15		07:23:01.84	−14:41:32.8	0.221 ± 0.014	−1.34 ± 0.70	0.81 ± 0.70	47 ± 10	Per	28
G232.62+00.99		07:32:09.78	−16:58:12.8	0.596 ± 0.035	−2.17 ± 0.38	2.09 ± 0.60	21 ± 3	Loc	40
G236.81+01.98		07:44:28.24	−20:08:30.2	0.298 ± 0.018	−3.10 ± 0.63	2.12 ± 0.63	43 ± 7	Per	28
G239.35−05.06	VY CMa	07:22:58.33	−25:46:03.1	0.855 ± 0.057	−2.80 ± 0.58	2.60 ± 0.58	20 ± 3	Loc	46, 47
G240.31+00.07		07:44:51.92	−24:07:41.5	0.212 ± 0.021	−2.36 ± 0.23	2.45 ± 0.30	67 ± 5	Per	28

Notes. Columns 1 and 2 give the Galactic source name/coordinates and an alias, when appropriate. Right ascension and declination (J2000) are listed in Columns 3 and 4. Columns 5–7 give the parallax and proper motion in the eastward ($\mu_x = \mu_\alpha \cos\delta$) and northward directions ($\mu_y = \mu_\delta$). Column 8 lists local standard of rest velocity. Column 9 indicates the spiral arm in which it resides, based mostly on association with structure seen in ℓ–V plots of CO and H I emission (not using the measured parallaxes); starting at the Galactic center and moving outward, Con = Connecting arm, 3 − k = 3 kpc arm, 4 − k = 4 kpc/Norma arm, Sct = Scutum-Crux-Centaurus arm, Sgr = Sagittarius arm, Loc = Local arm, Per = Perseus arm, and Out = Outer arm; a few sources, indicated with "..." could not be confidently assigned to an arm. Some parameter values listed here were preliminary ones and may be slightly different from final values appearing in published papers. Motion components and their uncertainties are meant to reflect that of the central star that excites the masers, and may be larger than formal measurement uncertainties quoted in some papers. Parallax uncertainties for sources with multiple (N) maser spots have been adjusted upward by $\sqrt{N}$, if not done so in the original publications.

References. (1) BeSSeL Survey unpublished; (2) Wu et al. 2014; (3) Reid et al. 2009c; (4) Sato et al. 2014; (5) Sanna et al. 2009; (6) Zhang et al. 2014; (7) Sanna et al. 2014; (8) Immer et al. 2013; (9) Sato et al. 2010a; (10) Xu et al. 2011; (11) Brunthaler et al. 2009; (12) Bartkiewicz et al. 2008; (13) Kurayama et al. 2011; (14) Zhang et al. 2009; (15) Zhang et al. 2013; (16) Xu et al. 2009; (17) Sato et al. 2010b; (18) Oh et al. 2010; (19) Rygl et al. 2010; (20) Nagayama et al. 2011; (21) Xu et al. 2013; (22) Sanna et al. 2012; (23) Ando et al. 2011; (24) Moscadelli et al. 2011; (25) Rygl et al. 2012; (26) Zhang et al. 2012b; (27) Hachisuka et al. 2014; (28) Choi et al. 2014; (29) Hirota et al. 2008; (30) Moscadelli et al. 2009; (31) Moellenbrock et al. 2009; (32) Sato et al. 2008; (33) Xu et al. 2006; (34) Hachisuka et al. 2006; (35) Asaki et al. 2010; (36) Hachisuka et al. 2009; (37) Hachisuka et al. 2014; (38) Honma et al. 2011; (39) Niinuma et al. 2011; (40) Reid et al. 2009a; (41) Shiozaki et al. 2011; (42) Honma et al. 2007; (43) Sandstrom et al. 2007; (44) Menten et al. 2007; (45) Kim et al. 2008; (46) Choi et al. 2008; (47) Zhang et al. 2012a.

(This table is also available in a machine-readable form in the online journal.)

The sum of the squares of the residuals divided by their uncertainties in the y_r direction were minimized. Since preliminary estimates of ψ affect these quantities, we iterated the fitting to convergence. Final parameter values were estimated from marginalized posteriori probability density distribution functions (PDFs) for each parameter based on McMC trials that were accepted or rejected following the Metropolis–Hastings algorithm; the values reported in Table 2 assume $R_0 = 8.34$ kpc (see Section 4). Based on the fitted parameter values, we plot the trace of the centers and 1σ widths of each arm on Figure 1.

The intrinsic widths of the spiral arms, estimated from the a_w parameters, show an interesting pattern in Figure 2. The estimated arm widths increase nearly linearly with Galactocentric radius at a rate of 42 pc kpc^{-1} between radii of 5–13 kpc.

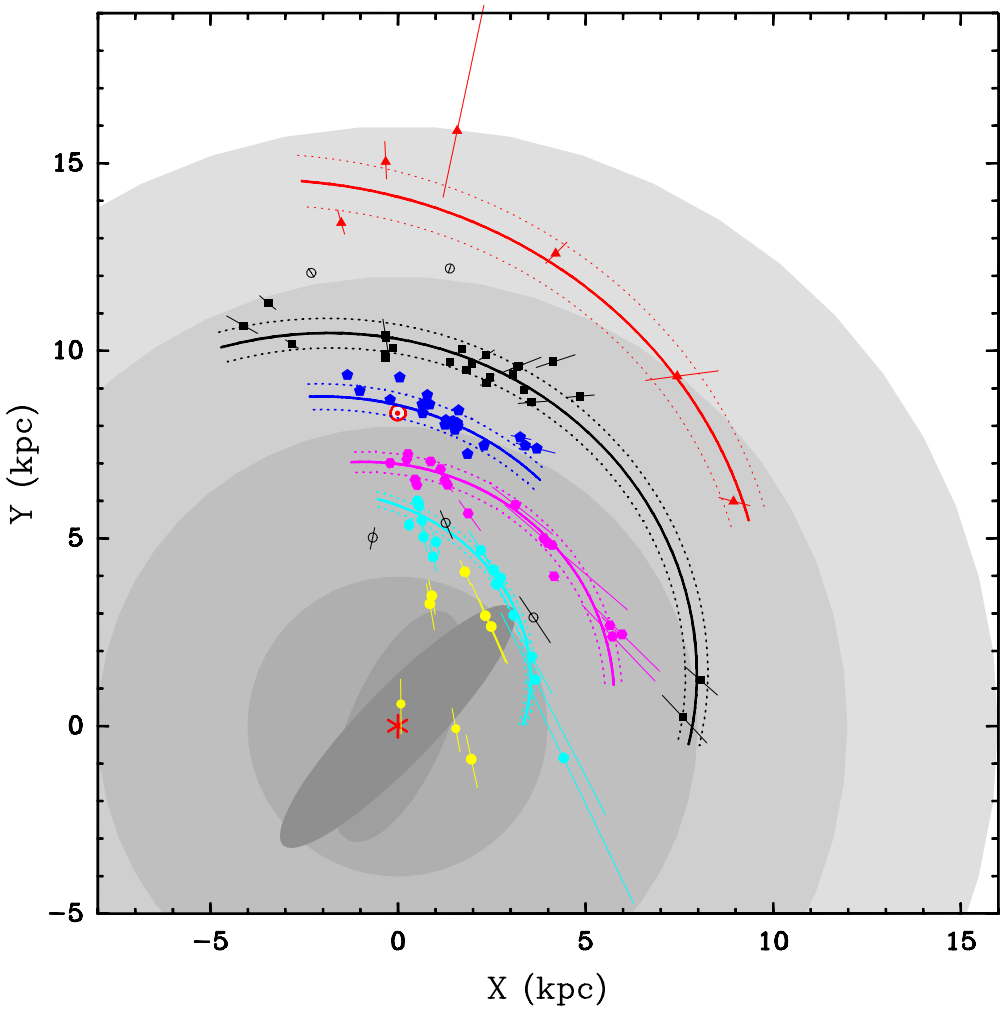

Figure 1. Plan view of the Milky Way showing the locations of high-mass star forming regions (HMSFRs) with trigonometric parallaxes measured by the VLBA, VERA, and the EVN. The Galactic center (red asterisk) is at (0,0) and the Sun (red Sun symbol) is at (0,8.34). HMSFRs were assigned to spiral arms based primarily on association with structure seen in ℓ–V plots of CO and H I emission (and not based on the measured parallaxes): inner Galaxy sources, yellow dots; Scutum arm, cyan octagons; Sagittarius arm, magenta hexagons; Local arm, blue pentagons; Perseus arm, black squares; Outer arm, red triangles. Open circles indicate sources for which arm assignment was unclear. Distance error bars are indicated, but many are smaller than the symbols. The background gray disks provide scale, with radii corresponding in round numbers to the Galactic bar region (≈4 kpc), the solar circle (≈8 kpc), co-rotation of the spiral pattern and Galactic orbits (≈12 kpc), and the end of major star formation (≈16 kpc). The short COBE "boxy-bar" and the "long" bar (Blitz & Spergel 1991; Hammersley et al. 2000; Benjamin 2008) are indicated with shaded ellipses. The solid curved lines trace the centers (and dotted lines the 1σ widths) of the spiral arms from the log-periodic spiral fitting (see Section 3 and Table 2). For this view of the Milky Way from the north Galactic pole, Galactic rotation is clockwise.

(A color version of this figure is available in the online journal.)

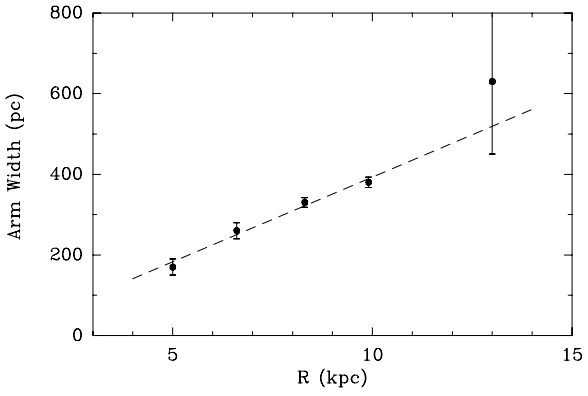

Figure 2. Spiral arm width increasing with Galactocentric radius. The dashed line is a variance-weighted fit with a slope of 42 pc kpc^{-1}. See Table 2 for details.

Spiral pitch angles vary between 7° and 20° as listed in Table 2. The significant range of pitch angles among arms suggests that no single value applies to all arms and, possibly, cannot be applied to the full length of an arm as it winds around the Galaxy (Savchenko & Reshetnikov 2013). However, these pitch angles are characteristic of spiral galaxies of Sb to Sc class (Kennicutt 1981), further supporting the identification of ℓ–V tracks as spiral arms for the Milky Way.

The HMSFRs with measured parallaxes are clearly tracing the major spiral arms of the Milky Way (see Figure 1), and details of the locations and properties of the individual arms can be found in the primary references (Hachisuka et al. 2014; Choi et al. 2014; Zhang et al. 2013; Xu et al. 2013; Wu et al. 2014; Sato et al. 2014; Sanna et al. 2014). Interestingly, some surprising results are already evident. We are finding that the Perseus arm, thought to be one of the major spiral arms of the

Table 2
Spiral Arm Characteristics

Arm	N	$\beta_{\rm ref}$ (β Range) (deg)	$R_{\rm ref}$ (kpc)	Width (kpc)	ψ (deg)
Scutum	17	27.6 (+3 → 101)	5.0 ± 0.1	0.17 ± 0.02	19.8 ± 2.6
Sagittarius	18	25.6 (−2 → 68)	6.6 ± 0.1	0.26 ± 0.02	6.9 ± 1.6
Local	25	8.9 (−8 → 27)	8.4 ± 0.1	0.33 ± 0.01	12.8 ± 2.7
Perseus	24	14.2 (−21 → 88)	9.9 ± 0.1	0.38 ± 0.01	9.4 ± 1.4
Outer	6	18.6 (−6 → 56)	13.0 ± 0.3	0.63 ± 0.18	13.8 ± 3.3

Notes. Spiral arm data from fitting a section of a log-periodic spiral for the arms listed in Column 1. See the primary papers for more information on each arm: Scutum arm (Sato et al. 2014), Sagittarius arm (Wu et al. 2014), Local arm (Xu et al. 2013), Perseus arm (Choi et al. 2014; Zhang et al. 2013), Outer arm (Hachisuka et al. 2014, in preparation). Small differences between parameter values in these papers and here reflect small differences between preliminary and final parallax values and the adopted value for R_0; here we use $R_0 \equiv 8.34$ kpc. For the Local arm, the pitch angle fit here used only HMSFRs. Column 2 lists the number of HMSFRs with parallax measurements used in the fits. Columns 3 and 4 give the reference Galactocentric azimuth, an arbitrary value assigned near the center of the range of source azimuths (given in parentheses), and the fitted radius at that azimuth. Column 5 is an estimate of the intrinsic arm width, based on the magnitude of "astrophysical noise" added to the measurement uncertainty to achieve a χ^2_ν per degree of freedom near unity. Column 6 is the spiral arm pitch angle, a measure of how tightly wound the spiral is.

Milky Way, has little massive star formation over a 6 kpc long arc between Galactic longitudes of 50° and 80° (Choi et al. 2014; Zhang et al. 2013). On the other hand, the Local (Orion) arm, often called a "spur" and considered a minor structure (Blaauw 1985), has comparable massive star formation to its adjacent Sagittarius and Perseus arms (Xu et al. 2013).

4. MODELING THE GALAXY

Given measurements of position, parallax, proper motion and Doppler shift, one has complete three-dimensional location and velocity vectors relative to the Sun. One can then construct a model of the Milky Way and adjust the model parameters to best match the data. As in Reid et al. (2009b), we model the Milky Way as a disk rotating with speed $\Theta(R) = \Theta_0 + (d\Theta/dR)(R - R_0)$, where R_0 is the distance from the Sun to the Galactic center and Θ_0 is the circular rotation speed at this distance. We then evaluate the effects of different forms for the rotation curve. Since all measured motions are relative to the Sun, we need to model the peculiar (non-circular) motion of the Sun, parameterized by $U_\odot$ toward the Galactic center, $V_\odot$ in the direction of Galactic rotation, and $W_\odot$ toward the north Galactic pole (NGP). Table 3 summarizes these and other parameters.

For each source, we treated the three-dimensional velocity components (two components of proper motion, μ_x and μ_y, and the heliocentric Doppler velocity, $v_{\rm Helio}$), as data to be compared to a model. The source coordinates (ℓ, b) and parallax distance ($1/\pi_s$) were treated as independent variables. This approach is slightly different than in Reid et al. (2009b), where the parallaxes were also treated as data in the least-squares fitting. While that approach adds some extra information (e.g., for sources near the Galactic tangent points, distance is very sensitive to Doppler velocity, but not vice versa), it brings correlated data into the fitting, which will lead to slightly underestimated parameter uncertainties. We tested the inclusion versus exclusion of parallax with simulated data sets and found little difference and no bias between the methods. However, in order to avoid the need to adjust formal parameter uncertainties, as well as subtle issues associated with resolving the near/far distance ambiguities for sources in the first and fourth Galactic quadrants, we used the more conservative "velocity-only" fitting as done, for example, by others (Bovy et al. 2009; McMillan & Binney 2010; Bobylev & Bajkova 2010; Honma et al. 2012).

Table 3
Galaxy Model Parameter Definitions

Parameter	Definition
R_0	Distance of Sun from GC
Θ_0	Rotation speed of Galaxy at R_0
$d\Theta/dR$	Derivative of Θ with R: $\Theta(R) = \Theta_0 + (d\Theta/dR)(R - R_0)$
$U_\odot$	Solar motion toward GC
$V_\odot$	Solar motion in direction of Galactic rotation
$W_\odot$	Solar motion toward NGP
$\overline{U_s}$	Average source peculiar motion toward GC
$\overline{V_s}$	Average source peculiar motion in direction of Galactic rotation
$\overline{W_s}$	Average source peculiar motion toward NGP

Notes. GC is the Galactic center and NGP is the north Galactic pole. The average source peculiar motions ($\overline{U_s}$,$\overline{V_s}$,$\overline{W_s}$) are defined at the location of the source and are rotated with respect to the solar motion ($U_\odot$,$V_\odot$,$W_\odot$) by the Galactocentric azimuth, β, of the source (see Figure 8 of Reid et al. 2009b). We solve for the magnitude of each velocity component, but the orientation of the vector for each source depends on location in the Galaxy.

4.1. Bayesian Fitting

We adjusted the Galactic parameters so as to best match the data to the spatial-kinematic model using a Bayesian fitting approach. The posteriori PDFs of the parameters were estimated with McMC trials that were accepted or rejected by the Metropolis–Hastings algorithm. While a simple axi-symmetric model for the Galaxy may be a reasonable approximation for the majority of sources, a significant minority of outliers are expected for a variety of well known reasons. For example, the gravitational potential of the Galactic bar (or bars), which extend 3–4 kpc from the Galactic center (Liszt & Burton 1980; Blitz & Spergel 1991; Hammersley et al. 2000; Benjamin et al. 2005) is expected to induce large non-circular motions for sources in its vicinity. Indeed, some of these sources show large peculiar motions, although based on a nearly flat rotation curve extrapolated inward from measurements outside this region (Sanna et al. 2014). Therefore, we removed the eight sources within 4 kpc of the Galactic center (i.e., excluding G000.67−00.03, G009.62+00.19, G010.47+00.02, G010.62−00.38, G012.02−00.03, G023.43−00.18, G023.70−00.19, G027.36−00.16) before model fitting.

In the Galaxy's spiral arms, super-bubbles created by multiple supernovae can accelerate molecular clouds to ≈20 km s^{-1} (Sato et al. 2008). It is probably not possible, prior to fitting, to determine which sources have been thus affected and are likely kinematically anomalous. Therefore, we initially used an "outlier-tolerant" Bayesian fitting scheme described by Sivia & Skilling (2006) as a "conservative formulation," which minimizes the effects of deviant points on estimates of the fitted parameters. For this approach, one maximizes

$$\sum_{i=1}^{N}\sum_{j=1}^{3} \ln\left((1 - e^{-R_{i,j}^2/2})/R_{i,j}^2\right),$$

where the weighted residual $R_{i,j} = (v_{i,j} - m_{i,j})/w_{i,j}$ (i.e., the data (v) minus model (m) divided by the uncertainty (w)

of the $i^{\rm th}$ of N sources and $j^{\rm th}$ velocity component). For large residuals, this formulation assigns a $1/R^2$ probability, compared to a Gaussian probability of $e^{-R^2/2}$ which vanishes rapidly. Thus, for example, a 5σ outlier has a reasonable (4%) probability with the outlier-tolerant approach, compared to $\approx 10^{-6}$ probability for Gaussian errors in the least-squares method, and will not be given excessive weight when adjusting parameters. Once the outliers were identified and removed, we assumed Gaussian data uncertainties and fitted data by maximizing

$$\sum_{i=1}^{N}\sum_{j=1}^{3} -R_{i,j}^2/2,$$

essentially least-squares fitting.

Our choice of weights (w) for the data in the model fitting process was discussed in detail in Reid et al. (2009b). We include both measurement uncertainty and the effects of random (Virial) motions of a massive young star (with maser emission) with respect to the average motion of the much larger and more massive HMSFR when weighting the differences between observed and modeled components of motion. Specifically the proper motion and Doppler velocity weights were given by $w(\mu) = \sqrt{\sigma_\mu^2 + \sigma_{\rm Vir}^2/d_s^2}$ and $w(v_{\rm Helio}) = \sqrt{\sigma_v^2 + \sigma_{\rm Vir}^2}$, where $\sigma_{\rm Vir}^2$ is the expected (one-dimensional) Virial dispersion for stars in an HMSFR. We adopted $\sigma_{\rm Vir} = 5$ km s^{-1}, appropriate for HMSFRs with $\sim 10^4$ $M_\odot$within a radius of ~ 1 pc, and did not adjust this value. As will be seen in Section 4.1, the vast majority of the velocity data can be fit with a χ_ν^2 near unity with these weights. Note that we were fairly conservative when assigning motion uncertainties for individual stars based on the maser data (see Section 2), and this may result in a slightly low $\sigma_{\rm Vir}$ value in order to achieve unity χ_ν^2 fits.

4.2. Priors

In order to model the observations, one needs prior constraints on the non-circular motion of our measurement "platform" (i.e., the solar motion parameterized by $U_\odot$, $V_\odot$, $W_\odot$) and/or the average peculiar motion of the sources being measured (parameterized by $\overline{U_s}$, $\overline{V_s}$, $\overline{W_s}$). Allowing for a non-zero average source peculiar motion can be thought of as a first approximation of the kinematic effects of spiral structure. In Reid et al. (2009b), we assumed the solar motion determined by Dehnen & Binney (1998) based on *Hipparcos* measurements and concluded that HMSFRs lagged circular orbital speeds by 15 km s^{-1} (i.e., $\overline{V_s} = -15$ km s^{-1}). The observed orbital lag ($\overline{V_s} < 0$) is insensitive to the value adopted for Θ_0, but it is strongly correlated with the adopted solar motion component, $V_\odot$ (Reid et al. 2009b; Honma et al. 2012). Recently, the value of the solar motion component in the direction of Galactic rotation ($V_\odot$) has become controversial. Motivated in part by the large $\overline{V_s}$ lag in Reid et al. (2009b), Schoenrich et al. (2010) re-evaluated the standard "asymmetric-drift" approach used by Dehnen & Binney (1998) and concluded that it was biased by coupled metallicity/orbital-eccentricity effects. They suggested new solar motion values; specifically they argued for a substantial increase for $V_\odot$ from 5 to 12 km s^{-1}. This change would decrease the average orbital lag of HMSFRs ($\overline{V_s}$) by ≈ 7 km s^{-1} to a more theoretically appealing value near 8 km s^{-1}.

Based on the first year of data from the Apache Point Observatory Galactic Evolution Experiment (APOGEE), Bovy et al. (2012) argue that the Sun's motion relative to a circular orbit in the Galaxy (i.e., a "rotational standard of rest") is 26 km s^{-1} in the direction of Galactic rotation, suggesting that the entire solar neighborhood, which defines the LSR, leads a circular orbit by 14 km s^{-1}. Taking into account these developments, we considered a conservative prior of $V_\odot = 15 \pm 10$ km s^{-1}, that encompasses the values of $V_\odot$ from 5 to 26 km s^{-1} within approximately the $\pm 1\sigma$ range.

One could argue on theoretical grounds that HMSFRs should, on average, lag circular orbits by only a few km s^{-1} (McMillan & Binney 2010). We observe masers in HMSFRs that are very young and the gas out of which their exciting stars formed could have responded to magnetic shocks when entering spiral arms, leading to departures from circular speeds by $\lesssim 10$ km s^{-1} (Roberts & Yuan 1970), apportioned between components counter to rotation and toward the Galactic center. In addition, radial pressure gradients can also reduce orbital speeds of gas slightly (Burkert et al. 2010), contributing to a small lag of ≈ 1 km s^{-1}. Allowing for such effects, we consider priors for $\overline{U_s}$ of 3 ± 10 km s^{-1} and $\overline{V_s}$ of -3 ± 10 km s^{-1} as reasonable and conservative.

Given the current uncertainty in (1) the value for the circular ($V_\odot$) component of solar motion and (2) the magnitude of the average peculiar motions of HMSFRs, we tried four sets of priors when fitting the data:

Set-A. Adopting a loose prior for the $V_\odot$ component of solar motion, $U_\odot = 11.1 \pm 1.2$, $V_\odot = 15 \pm 10$, $W_\odot = 7.2 \pm 1.1$ km s^{-1}, and for the average peculiar motions for HMSFRs of $\overline{U_s} = 3 \pm 10$ and $\overline{V_s} = -3 \pm 10$ km s^{-1}.

Set-B. Using no priors for the average peculiar motions of HMSFRs, but tighter priors for the solar motion of $U_\odot = 11.1 \pm 1.2$, $V_\odot = 12.2 \pm 2.1$, $W_\odot = 7.2 \pm 1.1$ km s^{-1} from Schoenrich et al. (2010).

Set-C. Using no priors for the solar motion, but tighter priors on the average peculiar motions of HMSFRs of $\overline{U_s} = 3 \pm 5$ and $\overline{V_s} = -3 \pm 5$ km s^{-1}.

Set-D. Using essentially no priors for either the solar or average peculiar motions of HMSFRs, but bounding the $V_\odot$ and $\overline{V_s}$ parameters with equal probability within ± 20 km s^{-1} of the Set-A initial values and zero probability outside that range.

4.3. Models A1–A4

Using the 95 sources with Galactocentric radii greater than 4 kpc.[11] the outlier-tolerant Bayesian fitting approach, and the Set-A priors as described above, we obtained the parameter estimates listed in Table 4 under fit A1. As expected for a sample with some outliers (see discussion in Section 4.1), we found a $\chi^2 = 562.6$, greatly exceeded the 277 degrees of freedom, owing to a number of sources with large residuals.

We iteratively removed the sources with the largest residuals. Using the outlier-tolerant Bayesian fitting approach (see Section 4.1) minimizes potential bias, based on assumed "correct" parameter values, when editing data. However, to further guard against any residual bias, we first removed sources with $>6\sigma$ residuals, followed by re-fitting and removal of those with $>4\sigma$ residuals, and finally re-fitting and removal of

[11] Removing sources for which $R < 4$ kpc: G000.67 − 00.03, G009.62 + 00.19, G010.47 + 00.02, G010.62 − 00.38, G012.02 − 00.03, G023.43 − 00.18, G023.70 − 00.19, G027.36 − 00.16.

Table 4
Bayesian Fitting Results

	A1	A5	B1	C1	D1
Parameter Estimates					
R_0(kpc)	8.15 ± 0.25	8.34 ± 0.16	8.33 ± 0.16	8.30 ± 0.19	8.29 ± 0.21
Θ_0(km s^{-1})	238 ± 11	240 ± 8	243 ± 6	239 ± 8	238 ± 15
$\frac{d\Theta}{dR}$(km s^{-1} kpc^{-1})	-0.1 ± 0.7	-0.2 ± 0.4	-0.2 ± 0.4	-0.1 ± 0.4	-0.1 ± 0.4
$U_\odot$(km s^{-1})	10.4 ± 1.8	10.7 ± 1.8	10.7 ± 1.8	9.9 ± 3.0	9.6 ± 3.9
$V_\odot$(km s^{-1})	15.1 ± 7.3	15.6 ± 6.8	12.2 ± 2.0	14.6 ± 5.0	16.1 ± 13.5
$W_\odot$(km s^{-1})	8.2 ± 1.2	8.9 ± 0.9	8.7 ± 0.9	9.3 ± 1.0	9.3 ± 1.0
$\overline{U_s}$(km s^{-1})	3.7 ± 2.4	2.9 ± 2.1	2.9 ± 2.1	2.2 ± 3.0	1.6 ± 3.9
$\overline{V_s}$(km s^{-1})	-2.4 ± 7.4	-1.6 ± 6.8	-5.0 ± 2.1	-2.4 ± 5.0	-1.2 ± 13.6
Fit statistics					
χ^2	562.6	224.9	225.1	224.7	224.1
$N_{\rm dof}$	277	232	232	232	232
$N_{\rm sources}$	95	80	80	80	80
r_{R_0,Θ_0}	0.61	0.46	0.74	0.66	0.44

Notes. Fit A1 used the 95 sources in Table 1 for which Galactocentric radii exceeded 4 kpc, an "outlier tolerant" probability distribution function for the residuals (see Section 4.1), and Set-A priors: Gaussian solar motion priors of $U_\odot = 11.1 \pm 2.0$, $V_\odot = 15 \pm 10$, $W_\odot = 7.2 \pm 2.0$ km s^{-1} and average source peculiar motion priors of $\overline{U_s} = 3 \pm 10$ and $\overline{V_s} = -3 \pm 10$ km s^{-1}. Fit A5 removed 15 sources found in fit A1 to have a motion component residual greater than 3σ, used a Gaussian probability distribution function for the residuals (i.e., least-squares), and the same priors as A1. Fits B1, C1 and D1 were similar to A5, except for the priors: B1 used the solar motion priors of Schoenrich et al. (2010) ($U_\odot = 11.1 \pm 2.0$, $V_\odot = 12.2 \pm 2.1$, $W_\odot = 7.2 \pm 2.0$) km s^{-1} and no priors for source peculiar motions; C1 used no solar motion priors and source peculiar motion priors of $\overline{U_s} = 3 \pm 5$ and $\overline{V_s} = -3 \pm 5$ km s^{-1}; and D1 used flat priors for all parameters except $V_\odot^{\rm Std}$ and $\overline{V_s}$, which were given unity probability between ± 20 km s^{-1} of the initial Set-A values and zero probability outside this range. The fit statistics listed are chi-squared (χ^2), the number of degrees of freedom ($N_{\rm dof}$), the number of sources used ($N_{\rm sources}$), and the Pearson product-moment correlation coefficient for parameters R_0 and Θ_0 (r_{R_0,Θ_0}).

those with $>3\sigma$ residuals (fits A2, A3 and A4, not listed here). In total, 15 sources[12] were removed.

4.4. Model A5

With the resulting "clean" data set of 80 sources, we performed a least-squares fit (assuming a Gaussian PDF for the data uncertainties). We used the same loose priors (Set-A) as for model A1, namely solar motion components $U_\odot = 11.1 \pm 1.2$, $V_\odot = 15 \pm 10$, $W_\odot = 7.2 \pm 1.1$ km s^{-1} and average peculiar motions for HMSFRs of $\overline{U_s} = 3 \pm 10$ and $\overline{V_s} = -3 \pm 10$ km s^{-1}. This resulted in the parameter estimates listed under fit A5 in Table 4. This model produced a good $\chi^2 = 224.9$ for 232 degrees of freedom and estimates of $R_0 = 8.34 \pm 0.16$ kpc and $\Theta_0 = 240 \pm 8$ km s^{-1}. We find $d\Theta/dR = -0.2 \pm 0.4$ km s^{-1} kpc^{-1}, indicating a very flat rotation curve for the Milky Way between radii of $\approx$5 and 16 kpc from the Galactic center.

Compared to the preliminary results of Reid et al. (2009b) based on 16 sources, where the Pearson product-moment correlation coefficient for R_0 and Θ_0 was high, $r_{R_0,\Theta_0} = 0.87$, with the larger number of sources and a better distribution across the Galaxy, these parameters are significantly less correlated, $r_{R_0,\Theta_0} = 0.46$. The joint and marginalized PDFs for these fundamental Galactic parameters are displayed in Figure 3.

The circular velocity parameters are still correlated (see Section 4.10), but linear combinations of these parameters are

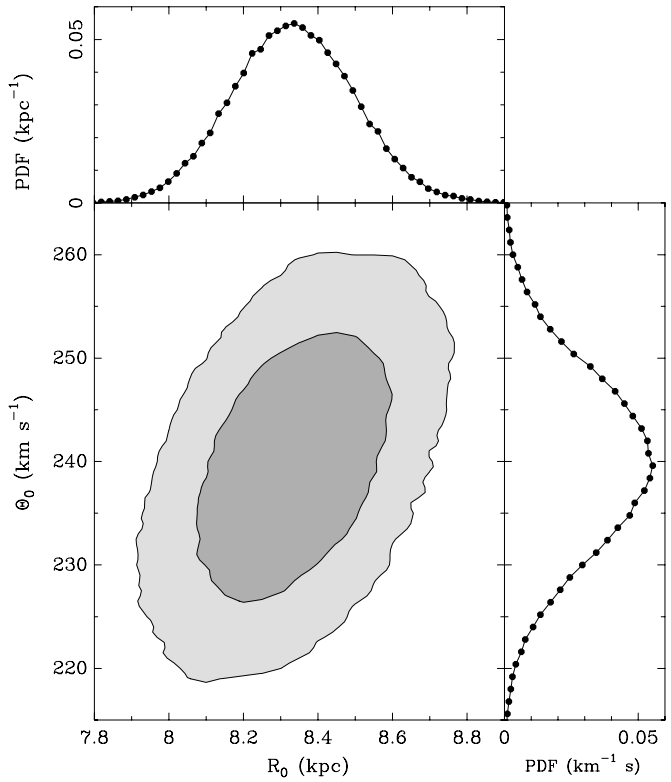

Figure 3. Joint and marginalized posteriori probability density distributions for R_0 and Θ_0 for model fit A5. Priors for the solar motion were $U_\odot = 11.1 \pm 1.2$, $V_\odot = 15 \pm 10$, $W_\odot = 7.2 \pm 1.1$ km s^{-1} and for the average peculiar motions for HMSFRs were $\overline{U_s} = 3 \pm 10$ and $\overline{V_s} = -3 \pm 10$ km s^{-1}. Contours enclose 95% and 68% probabilities. The Pearson product-moment correlation coefficient for R_0 and Θ_0 is 0.46.

[12] Removing outlying sources: G012.68−00.18, G016.58−00.05, G023.65−00.12, G025.70+00.04, G028.86+00.06, G029.95−00.01, G031.28+00.06, G033.64−00.22, G034.39+00.22, G078.12+03.63, G108.59+00.49, G111.54+0.77, G122.01−07.08, G133.94+01.06, G176.51+00.20.

well determined: $\Theta_0 + V_\odot = 255.2 \pm 5.1$ and $V_\odot - \overline{V_s} = 17.1 \pm 1.0$. Also, the angular rotation rate for the Sun's orbit about the Galactic center is constrained to $\pm 1.4\%$ accuracy: $(\Theta_0 + V_\odot)/R_0 = 30.57 \pm 0.43$ km s^{-1} kpc^{-1}. This value is consistent with the reflex of the *apparent* motion of Sgr A*, the assumed motionless supermassive black hole at the center of the Galaxy, which gives 30.26 ± 0.12 km s^{-1} kpc^{-1} (Reid & Brunthaler 2004).

The component of solar motion in the direction of Galactic rotation, $V_\odot$, estimated to be 15.6 ± 6.8 km s^{-1} is better constrained than the prior of 15 ± 10 km s^{-1}. It is consistent with the *local* estimate (relative to solar neighborhood stars) of 12 km s^{-1} (Schoenrich et al. 2010) and the *global* estimate of Bovy et al. (2012) of 26 ± 3 km s^{-1} (relative to stars across the Milky Way).

4.5. Model B1

In order to explore the sensitivity of the modeling to our priors, we fit the clean data set using the Set-B priors: adopting the latest *Hipparcos* measurement of the solar motion of $U_\odot = 11.1 \pm 1.2$, $V_\odot = 12.2 \pm 2.1$, $W_\odot = 7.2 \pm 1.1$ km s^{-1} (Schoenrich et al. 2010) and no prior information on the average peculiar motion of the HMSFRs. This resulted in parameter estimates similar to those of model A5, e.g., $R_0 = 8.33 \pm 0.16$ kpc and $\Theta_0 = 243 \pm 6$ km s^{-1}. The quality of fit, as measured by $\chi^2 = 225.1$ for 232 degrees of freedom, was comparably good as for model A5. The average velocity lag of the HMSFRs relative to circular orbits, which was not constrained by priors, was $\overline{V_s} = -5.0 \pm 2.1$ km s^{-1}. This is comparable to that found by Reid et al. (2009b), after correcting for the 7 km s^{-1} difference in the adopted solar motion values.

4.6. Model C1

Given the current uncertainty in the $V_\odot$ component of solar motion, we fit the data with the Set-C priors, assuming no prior information for the solar motion, but using a stronger prior than for model A5 for the average peculiar motion of the HMSFRs: $\overline{U_s} = 3 \pm 5$ and $\overline{V_s} = -3 \pm 5$ km s^{-1}. As for model B1, we found most parameter estimates to be similar to model A5, e.g., $R_0 = 8.30 \pm 0.19$ kpc and $\Theta_0 = 239 \pm 8$ km s^{-1}. For the solar motion, we find $U_\odot = 9.9 \pm 2.0$, $V_\odot = 14.6 \pm 5.0$, and $W_\odot = 9.3 \pm 1.0$ km s^{-1}. The $V_\odot$ value is consistent with revised Schoenrich et al. (2010; 12 km s^{-1}) solar motion, but differs by 2σ from the Bovy et al. (2012) estimate.

4.7. Model D1

In order to facilitate the use of the results presented here with other Galactic parameter estimates, we performed a fit with essentially no informative priors. We did this by taking the A5 (Set-A) initial parameter values and assuming flat priors for all parameters except for $V_\odot$ and $\overline{V_s}$. For these parameters we assumed equal probability for values within ± 20 km s^{-1} of the initial values and zero probability outside this range in order to exclude unreasonable parameter values. The parameters that remain well determined include $R_0 = 8.29 \pm 0.21$ kpc, $\Theta_0 = 238 \pm 15$ km s^{-1}, $d\Theta/dR = -0.1 \pm 0.4$ km s^{-1} kpc^{-1}, $U_\odot = 9.6 \pm 3.9$ km s^{-1}, $W_\odot = 9.3 \pm 1.0$ km s^{-1}, and $\overline{U_s} = 1.6 \pm 3.9$ km s^{-1}. The correlated velocity terms, $V_\odot$ and $\overline{V_s}$ displayed nearly flat posteriori PDFs over their allowed ranges. However, linear combinations involving these parameters are very well constrained, $\Theta_0 + V_\odot = 253.8 \pm 6.4$ km s^{-1} and $V_\odot - \overline{V_s} = 17.2 \pm 1.2$ km s^{-1}, as well as the angular rotation rate of the Sun about the Galactic center, $(\Theta_0 + V_\odot)/R_0 = 30.64 \pm 0.41$ km s^{-1} kpc^{-1}.

4.8. Rotation Curves

Next, we investigated the sensitivity of the fundamental Galactic parameters, R_0 and Θ_0, to alternative rotation curves. When fitting, we replaced the simple linear form, $\Theta(R) = \Theta_0 + (d\Theta/dR)(R - R_0)$, with the empirically determined functions of $\Theta(R)$ of Clemens (1985), the power-law parameterization of Brand & Blitz (1993), a polynomial, and the "universal" rotation curve of Persic et al. (1996). We adopted the Set-A priors in order to facilitate comparisons with the A5 fit. Table 5 presents the fitting results for these rotation curves.

Clemens (1985) supplied two curves with different shapes: one assuming the old IAU constants (C-10) of $R_0 = 10$ kpc and $\Theta_0 = 250$ km s^{-1} and the other assuming the revised constants (C-8.5) of $R_0 = 8.5$ kpc and $\Theta_0 = 220$ km s^{-1} currently in widespread use. The C-10 model has rotational speeds that rise faster with radius than the C-8.5 model. For either model, we fitted for different values of R_0 (which we used to scale model radii) and Θ_0 (which we used to scale rotation speeds).

Brand & Blitz (1993) parameterize their rotation curve (BB) as a power law in Galactocentric radius, R, with potentially three adjustable parameters: $\Theta(R) = a_1(R/R_0)^{a_2} + a_3$. For a flat rotation curve ($a_2 = 0$), parameters a_1 and a_3 become degenerate. Since the Galaxy's rotation curve is nearly flat over the range of radii we sample (see, e.g., model A5 above), we held a_3 at zero, solving only for a_1 and a_2. Indeed, we find the power law exponent, $a_2 = -0.01 \pm 0.01$, essentially flat. For this formulation, $a_1 = \Theta_0$, and in Table 5 we copy a_1 to Θ_0 to facilitate comparison with other models.

As an alternative to a power law rotation curve, we fitted a second-order polynomial (Poly) in $\rho = (R/R_0) - 1$: $\Theta(R) = a_1 + a_2\rho + a_3\rho^2$. The model fit parameters for this form of a rotation curve are similar to those from models C-10, BB and Univ.

The universal (Univ) rotation curve of Persic et al. (1996) includes terms for an exponential disk and a halo. It can have three adjustable parameters: a_1, the circular rotation speed at the radius enclosing 83% of the optical light ($R_{\rm opt}$); $a_2 = R_{\rm opt}/R_0$; and a_3, a core-radius parameter for the halo contribution, nominally 1.5 for an L^* galaxy. With flat priors for the three rotation curve parameters, the posteriori PDF for a_2 was bimodal, with the dominant peak at $a_2 = 0.9$ and a second peak with 50% of the primary's amplitude at $a_2 = 0.1$. Since the secondary peak seems unlikely, we refit the data using a prior for a_2 of 1.2 ± 0.5. We then obtained similar parameter values as other models (see Table 5), with the three adjustable rotation curve parameters of $a_1 = 241 \pm 8$ km s^{-1}, $a_2 = 0.90 \pm 0.06$, and $a_3 = 1.46 \pm 0.16$.

All but one of the rotation curve models lead to similar values for the fundamental Galactic parameters R_0 and Θ_0 as our A5 fit. Only the Clemens "$R_0 = 8.5$ kpc; $\Theta_0 = 220$ km s^{-1}" (C-8.5) rotation curve results in a marginally significant change in estimates of R_0 and Θ_0. However, this fit has a significantly poorer quality ($\chi^2 = 248.1$ for 233 degrees of freedom) than, for example, the A5 fit ($\chi^2 = 224.9$ for 232 degrees of freedom), and we do not consider this model further. We conclude that the fundamental Galactic parameters R_0 and Θ_0 are reasonably insensitive to a wide variety of rotation curve shapes.

With full three-dimensional location and velocity information, we can transform our heliocentric velocities to a

Table 5
Rotation Curve Results

	C-10	C-8.5	BB	Poly	Univ
Parameter Estimates					
R_0(kpc)	8.36 ± 0.16	8.12 ± 0.14	8.34 ± 0.16	8.34 ± 0.17	8.31 ± 0.16
Θ_0(km s^{-1})	237 ± 8	221 ± 8	240 ± 9	241 ± 9	241 ± 8
$U_\odot$(km s^{-1})	10.1 ± 1.8	10.5 ± 1.8	10.5 ± 1.8	10.7 ± 1.7	10.5 ± 1.7
$V_\odot$(km s^{-1})	19.4 ± 6.8	25.0 ± 6.8	15.5 ± 6.8	14.7 ± 6.8	14.4 ± 6.8
$W_\odot$(km s^{-1})	8.9 ± 1.0	8.9 ± 1.0	8.8 ± 1.0	8.8 ± 0.9	8.9 ± 0.9
$\overline{U_s}$(km s^{-1})	2.4 ± 2.1	2.6 ± 2.0	2.8 ± 2.0	2.8 ± 2.0	2.6 ± 2.1
$\overline{V_s}$(km s^{-1})	$+3.4 \pm 6.8$	$+8.5 \pm 6.8$	-1.5 ± 6.8	-1.4 ± 6.8	-1.4 ± 6.8
a_1(km s^{-1})	...	...	240 ± 9	241 ± 9	241 ± 8
a_2	...	...	0.00 ± 0.02	0.5 ± 3.7	0.90 ± 0.06
a_3	...	...	...	-15.1 ± 8.4	1.46 ± 0.16
Fit statistics					
χ^2	229.7	248.1	225.2	221.9	214.5
$N_{\rm dof}$	233	233	231	230	230
$N_{\rm sources}$	80	80	80	80	80
r_{R_0,Θ_0}	0.46	0.36	0.48	0.47	0.47

Notes. Rotation curves C-10 and C-8.5 are from Clemens (1985) for old and revised IAU recommended values of ($R_0 = 10$ kpc, $\Theta_0 = 250$ km s^{-1}) and ($R_0 = 8.5$ kpc, $\Theta_0 = 220$ km s^{-1}), respectively. These curves have been scaled by the fitted values for these fundamental parameters. Note the higher χ^2 value for the C-8.5 model compared to the others in the table. The "BB" rotation curve from Brand & Blitz (1993) is a power law in radius: $\Theta(R) = a_1(R/R_0)^{a_2}$. The "Poly" model is second-order polynomial in radius: $\Theta(R) = a_1 + a_2\rho + a_3\rho^2$, where $\rho = (R/R_0) - 1$. The "Univ" curve is a universal rotation curve (Persic et al. 1996), where a_1 is the rotation speed at the optical (83% light) radius, and the other parameters are dimensionless and provide the shape. For the latter three models, Θ_0 is not an independently adjustable parameter; instead it is calculated from a_1, a_2, and a_3.

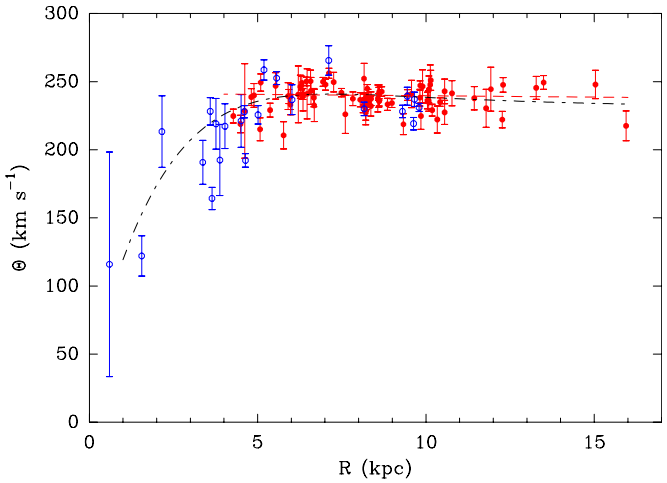

Figure 4. Rotation curve for all high mass star forming regions with measured parallax and proper motion in Table 1. Plotted is the circular velocity component, Θ, as a function of Galactocentric radius, R. The transformation from heliocentric to Galactocentric frames uses the parameter values of fit A5, based only on sources with $R > 4.0$ kpc; these sources are plotted with filled red symbols. The sources not used in the final fitting are plotted with open blue symbols. The dashed red line indicates the fitted rotation curve (model A5) given by $\Theta = \Theta_0 - 0.2(R - R_0)$ km s^{-1}, where R and R_0 are in kpc. The dash-dot black line is the best fit "universal" rotation curve (model D1) for spiral galaxies (Persic et al. 1996), which begins to capture the clear velocity turn down for stars with $R \lesssim 5.0$ kpc.

(A color version of this figure is available in the online journal.)

Galactocentric reference frame and calculate the tangential (circular) speed for each HMSFR. Figure 4 plots these speeds for *all* sources in Table 1. Most published rotation curves for the Milky Way have come from only one component of velocity (radial), often using kinematic distances and *assuming* a value for Θ_0. As such, the data in Figure 4 represent a considerable advance. See also the analysis of this data set by Xin & Zheng (2013).

It is important to remember that the transformation from heliocentric to Galactocentric frames requires accurate values of R_0, $U_\odot$, and, most importantly, $\Theta_0 + V_\odot$, since the motion of the Sun has (by definition) been subtracted in the heliocentric frame. For most sources, increasing or decreasing the assumed value of $\Theta_0 + V_\odot$ would, correspondingly, move each data point up or down by about the same amount. Thus, the level of this, and essentially all published, rotation curves is determined mostly by $\Theta_0 + V_\odot$. Our results are the first to use fully three-dimensional data to strongly constrain all three parameters: R_0, $U_\odot$ and $\Theta_0 + V$.

The dashed line in Figure 4 represent the linear rotation curve from the A5 fit, based only on sources with $R > 4$ kpc. Sources used in the fit are plotted with filled symbols and the sources not used with open symbols. The dashed line indicates the expected rotation for sources in circular Galactic orbit (i.e., $\overline{U_s} = \overline{V_s} = 0$). There are now sufficient data to clearly indicate that the rotation curve drops at Galactocentric radii $\lesssim$4 kpc. However, given the likelihood for a significant non-axisymmetric gravitational potential within $\approx$4 kpc of the center, more measurements are needed before extending a rotation curve to this region as azimuthal terms may be needed.

4.9. Peculiar Motions of HMSFRs

Figure 5 shows the peculiar (non-circular) motions of all sources in Table 1 with motion uncertainties less than 20 km s^{-1}. Similar results were described in the primary papers presenting the parallaxes and proper motions for each arm (Sato et al. 2014; Wu et al. 2014; Xu et al. 2013; Choi et al. 2014; Zhang et al. 2013; Hachisuka et al. 2014). For uniformity, here the motions were calculated using the A5 fit parameters (see Table 4), but with zero correction for the average source peculiar

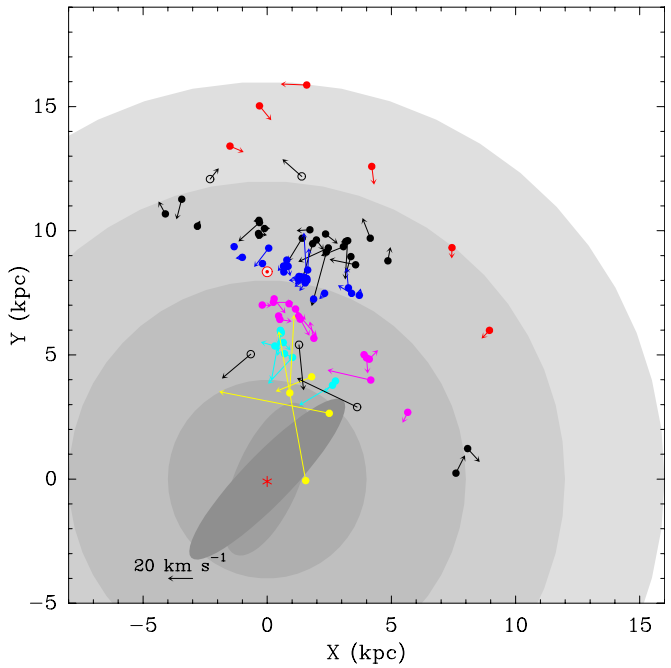

Figure 5. Peculiar (non-circular) motions of HMSFRs projected on the Galactic plane. These motions (arrows) were calculated with parameter values from the A5 fit, specifically $R_0 = 8.34$ kpc, $\Theta_0 = 240$ km s^{-1}, $d\Theta/dR = -0.2$ km s^{-1} kpc^{-1}, and $U_\odot = 10.7$, $V_\odot = 15.6$ km s^{-1} (but without correction for $\overline{U_s}$ or $\overline{V_s}$). Only sources with motion uncertainties <20 km s^{-1} are plotted. A 20 km s^{-1} scale vector is shown at the bottom left. Spiral arm sources are color coded as describe in Figure 1. The Galaxy rotates clockwise on this view from the NGP.

(A color version of this figure is available in the online journal.)

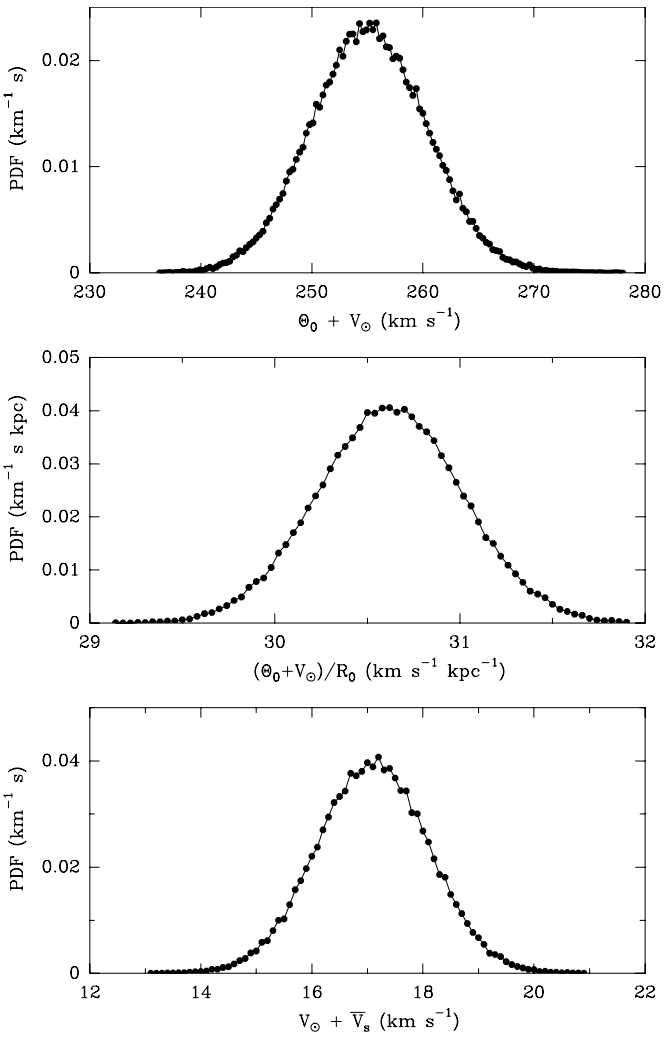

Figure 6. Marginalized posteriori probability density distributions for correlated circular velocity parameters from fit A5. Top panel: the circular orbital speed of the Sun: $\Theta_0 + V_\odot$. Middle panel: the angular orbital speed of the Sun: $(\Theta_0 + V_\odot)/R_0$. Bottom panel: difference between the circular solar and average source peculiar motions: $V_\odot - \overline{V_s}$.

motions. Typical peculiar motions are ≈10 km s^{-1}, but some sources have much larger values. For example, many sources in the Perseus arm in the Galactic longitude range ≈100° to ≈135° display peculiar motions ≳20 km s^{-1}. Many sources within ≈4 kpc of the Galactic center display even larger peculiar motions, probably indicating that the rotation curve used here is inadequate to describe their Galactic orbits, especially in the presence of the Galactic bar(s).

4.10. Parameter Correlations

The Pearson product-moment correlation coefficients, r, for all parameters from fit A5 are listed in Table 6. In the preliminary analysis of 16 HMSFRs with parallaxes and proper motions of Reid et al. (2009b), the estimates of R_0 and Θ_0 were strongly correlated ($r_{R_0,\Theta_0} = 0.87$). However, with the much larger set of HMSFRs that covers a larger portion of the Galaxy, the correlation between R_0 and Θ_0 estimates is now moderate: $r_{R_0,\Theta_0} = 0.465$ for our reference A5 fit. However, there remains a significant anti-correlation between Θ_0 and $V_\odot$ ($r_{\Theta_0,V_\odot} = -0.809$), as well as a strong correlation between $V_\odot$ and $\overline{V_s}$ ($r_{V_\odot,\overline{V_s}} = 0.990$). As suggested by the fitted parameter values in Table 4, our data strongly constrain the following combinations of these correlated parameters: $\Theta_0 + V_\odot = 255.2 \pm 5.1$ km s^{-1} and $V_\odot - \overline{V_s} = 17.1 \pm 1.0$ km s^{-1}. Also, the combination of parameters that yield the angular orbital speed of the Sun about the Galactic center, $(\Theta_0+V_\odot)/R_0 = 30.57 \pm 0.43$ km s^{-1} kpc^{-1}, is more tightly constrained than the individual parameters. Figure 6 shows the marginalized PDFs for these combinations of parameters.

4.11. Comparison with Other Modeling Approaches

Other groups have analyzed parallax and proper motion data sets from the BeSSeL Survey and the VERA project, focusing on different assumptions and results. Bovy et al. (2009) confirmed the counter rotation of HMSFRs (assuming $V_\odot = 5$ km s^{-1}) noted by Reid et al. (2009b) and argued for a comparable value for Θ_0 (246 ± 30 km s^{-1}), but with considerably lower significance. Alternatively, McMillan & Binney (2010) found that the $V_\odot$-component of solar motion of 5 km s^{-1}, provided by Dehnen & Binney (1998), should be raised to ≈12 km s^{-1}, thereby reducing the estimated counter-rotation of HMSFRs. Bobylev & Bajkova (2010), using 28 parallaxes available at that time and a Fourier analysis technique, estimated $\Theta_0 = 248 \pm 14$ km s^{-1} and $V_\odot = 11.0 \pm 1.7$ km s^{-1}, assuming $R_0 \equiv 8.0$ kpc. Finally, Honma et al. (2012), using 52 parallaxes, including some low-mass star forming regions, estimated $R_0 = 8.05 \pm 0.45$ kpc and $\Theta_0 = 238 \pm 14$ km s^{-1} for $V_\odot \equiv 12$ km s^{-1}.

The Bovy et al. (2009) re-analysis of our preliminary data employed a different approach than that of Reid et al. (2009b). Bovy et al. treat the elements of the velocity dispersion tensor of the HMSFRs as free parameters. These parameters give the

Table 6
Parameter Correlation Coefficients

	R_0	Θ_0	$d\Theta/dR$	$U_\odot$	$V_\odot$	$W_\odot$	$\overline{U_s}$	$\overline{V_s}$
R_0	1.000	0.465	0.103	0.452	0.023	−0.003	0.517	−0.002
Θ_0	0.465	1.000	0.136	0.243	−0.796	−0.009	0.171	−0.809
$d\Theta/dR$	0.103	0.136	1.000	−0.124	−0.009	0.025	−0.094	−0.018
$U_\odot$	0.452	0.243	−0.124	1.000	−0.014	−0.017	0.839	0.025
$V_\odot$	0.023	−0.796	−0.009	−0.014	1.000	0.011	−0.006	0.990
$W_\odot$	−0.003	−0.009	0.025	−0.017	0.011	1.000	−0.002	0.010
$\overline{U_s}$	0.517	0.171	−0.094	0.839	−0.006	−0.002	1.000	0.028
$\overline{V_s}$	−0.002	−0.809	−0.018	0.025	0.990	0.010	0.028	1.000

Notes. Pearson product-moment correlation coefficients for the A5 fit calculated from 10^6 McMC trial parameter values thinned by a factor of 10. Parameter definitions are given in the text and the notes in Table 3.

expected deviations (variances and covariances) of the velocity data from a smooth, axi-symmetric model of Galactic rotation and are used to adjust the weights applied to the different velocity components when fitting the data. However, while Bovy et al. found a significant trace for the tensor, the velocity dispersion parameters were only marginally constrained; formally none of the diagonal components had $>2.8\sigma$ formal significance. Also, their values for the radial and tangential components were nearly identical, suggesting that little is gained by making these free parameters versus adopting a single physically motivated value ($\sigma_{\rm Vir}$) as we have done. Note that our value for $\sigma_{\rm Vir}$ is comparable to the dispersion parameter (Δ_v) values found by McMillan & Binney (2010), which range from about 6 to 10 km s^{-1}, but is considerably smaller than those of Bovy et al. (2009) of $\approx$20 km s^{-1}. The reason for this difference is unclear, but might reflect different treatments of outlying data and/or increased parameter correlations associated with the six extra parameters used in solving for the tensor elements.

5. DISCUSSION

5.1. Solar Motion

If one adopts the theoretically motivated prior that HMSFRs have small peculiar motions (Set-C with no prior on the solar motion), then model fit C1 indicates $V_\odot = 14.6 \pm 5.0$ km s^{-1}. This is a *global* measure of the peculiar motion of the Sun and, as such, is relative to a "rotational standard of rest" as opposed to an LSR, defined relative to stellar motions in the solar neighborhood. If solar neighborhood stars (extrapolated to a zero-dispersion sample) are, on average, stationary with respect to a circular orbit, then these two solar motion systems will be the same. Our estimate of $V_\odot$ is consistent with the 12 km s^{-1} value of Schoenrich et al. (2010), measured with respect to solar neighborhood stars, but there is some tension between our global estimate of $V_\odot$ and that of Bovy et al. (2012) of 26 ± 3 km s^{-1}, as these two estimates differ by about 2σ. However, if one drops the prior that HMSFRs have small peculiar motions, then our result loses significance.

The large counter-rotation of HMSFRs, originally suggested by Reid et al. (2009b), was based on the initial *Hipparcos* result of Dehnen & Binney (1998) that $V_\odot = 5$ km s^{-1}. As the outcome of the Schoenrich et al. (2010) re-analysis of *Hipparcos* data, which gives $V_\odot = 12$ km s^{-1}, supersedes that lower $V_\odot$ value, it now appears that any average counter-rotation of HMSFRs is $\lesssim$5 km s^{-1}. Given that we strongly constrain $V_\odot - \overline{V_s} = 17.1 \pm 1.0$ km s^{-1}, were one to independently constrain $V_\odot$ with ± 2 km s^{-1} accuracy, the issue of HMSFR counter rotation could be clarified.

While our estimate of $V_\odot$ has a large uncertainty (owing to correlations with Θ_0 and $\overline{V_s}$), we find $U_\odot$ and $W_\odot$ are well constrained. In fit D1, in which no informative prior was used for the components of motion either toward the Galactic center or perpendicular to the Galactic plane, we find that $U_\odot = 9.6 \pm 3.9$ and $W_\odot = 9.3 \pm 1.0$ km s^{-1}, respectively. Our estimate of the Sun's motion toward the Galactic center is in agreement with most other estimates, e.g., 11.1 ± 1.2 km s^{-1} by Schoenrich et al. (2010) and 10 ± 1 km s^{-1} by Bovy et al. (2012); see also the compilation of estimates by Coskunoglu et al. (2011).

The solar motion component perpendicular to the Galactic plane, $W_\odot$, is generally considered to be straight forwardly determined and recent estimates typically range between 7.2 km s^{-1} (Schoenrich et al. 2010; relative to local stars within $\sim$0.2 kpc) and 7.6 km s^{-1} (Feast & Whitelock 1997; relative to stars within $\sim$3 kpc), with uncertainties of about $\pm$0.5 km s^{-1}. We find a slightly larger value of $W_\odot = 9.3 \pm 1.0$ km s^{-1} (for model D1 which used no informative priors for the solar motion), which may be significant; the difference between the locally and our globally measured value (i.e., relative to stars across the Galaxy) is 2.1 ± 1.1 km s^{-1}. Note that one might expect a small difference between measurements with respect to a local and a global distribution of stars were the disk of the Galaxy to precess owing to Local Group torques. Simulations of galaxy interactions in a group suggest that a disk galaxy can complete one precession cycle over a Hubble time. Were the Milky Way to do this, one would expect a vertical precessional motion at a Galactocentric radius of the solar neighborhood of order $R_0 H_0 \sim 0.6$ km s^{-1}. It is possible that the differences in the local and global estimates of $W_\odot$ can, in part, be explained in this manner.

5.2. Galactic Rotation Curve and Disk Scale Length

Among the various forms of rotation curves that we fit to the data, the universal curve advocated by Persic et al. (1996) to apply to most spiral galaxies yielded the best fit (see discussion in Section 4.8, Table 5 and Figure 4). This rotation curve matches the flat to slightly declining run of velocity with Galactocentric radius from $R \approx 5 \rightarrow 16$ kpc, as well as reasonably tracing the decline in orbital velocity for $R \lesssim 5$ kpc. However, many of the sources near the Galactic bar(s) cannot be well modeled with any axi-symmetric rotation curve.

The best fit value for our a_2 parameter ($R_{\rm opt}/R_0$), coupled with our estimate of $R_0 = 8.34 \pm 0.16$, locates $R_{\rm opt}$ at 7.5 ± 0.52 kpc. The a_2 parameter is sensitive to the slope of the rotation curve (near $R_{\rm opt}$) and the radius at which it turns down toward the Galactic center. For example, setting $a_2 = 0.7$ steepens the rotation curve at large radii and moves the turn down radius to $\approx$3.5 kpc, while setting $a_2 = 1.1$ flattens the rotation curve

and increases the turn down radius to ≈6.5 kpc. Given that the (thin) disk scale length, $R_D = R_{\rm opt}/3.2$ (Persic et al. 1996), we estimate $R_D = 2.44 \pm 0.16$ kpc. Estimates of R_D in the literature range from ≈1 → 6 kpc (Kent et al. 1991; Chang et al. 2011; McMillan 2011), with most consistent with a value between 2 → 3 kpc. Our estimate is also consistent with that of Porcel et al. (1998) who modeled the positions and magnitudes of 700,000 stars in the Two Micron Galactic Survey database and found $R_D = 2.3 \pm 0.3$ kpc and, more recently, Bovy & Rix (2013), who modeled the dynamics of ≈16,000 stars from the SEGUE survey and concluded that $R_D = 2.14 \pm 0.14$ kpc.

5.3. The Distance to the Galactic Center: R_0

Models A5, B1 and C1, which used different combinations of solar motion and/or average source peculiar motion priors, have comparable χ^2 values and all parameter estimates are statistically consistent. Because the priors for Model A5 are the least restrictive in keeping with current knowledge, we adopt those parameters as representative. Specifically, we find $R_0 = 8.34 \pm 0.16$ kpc, $\Theta_0 = 240 \pm 8$ km s^{-1} and $d\Theta/dR = -0.2 \pm 0.4$ km s^{-1} kpc^{-1}. As noted in Sections 4.10 and 4.8, with the much larger data set now available, estimates of R_0 and Θ_0 are no longer strongly correlated and appear fairly insensitive to the assumed nature of the rotation curve. These parameter estimates are consistent with, but significantly better than, the preliminary values of $R_0 = 8.4 \pm 0.6$ kpc, $\Theta_0 = 254 \pm 16$ km s^{-1} and a nearly flat rotation curve reported in Reid et al. (2009b), based on parallaxes and proper motions of 16 HMSFRs and assuming $V_\odot = 5$ km s^{-1}, and $R_0 = 8.05 \pm 0.45$ kpc and $\Theta_0 = 238 \pm 14$ km s^{-1} from Honma et al. (2012), based on a sample of 52 sources and assuming $V_\odot = 12$ km s^{-1}.

While there are numerous estimates of the distance to the Galactic center in the literature (e.g., Reid 1993), here we only compare those based on direct distance measurements. A parallax for the water masers in Sgr B2, a star forming region projected less than 0.1 kpc from the Galactic center, indicates $R_0 = 7.9 \pm 0.8$ kpc (Reid et al. 2009c), consistent with, but considerably less accurate than, our current result. More competitive estimates of R_0 come from the orbits of "S-stars" about the supermassive blackhole Sgr A*. Combining the nearly two decades of data from the ESO NTT/VLT (Gillessen et al. 2009b) and Keck (Ghez et al. 2008) telescopes that trace more than one full orbit for the star S2 (aka S0-2), Gillessen et al. (2009a) conclude that $R_0 = 8.28 \pm 0.33$ kpc. Recently the Keck group, extending their time sequence of observations by only a few years, announced a value of $R_0 = 7.7 \pm 0.4$ kpc (Morris et al. 2012), in mild tension both with the Gillessen et al. (2009a) analysis and our parallax-based result. However, in the latest publication of the Keck group, Do et al. (2013) combined modeling of the distribution and space velocities of stars within the central 0.5 pc of the Galactic center with the stellar orbital result for star S0-2 (Ghez et al. 2008) and conclude that $R_0 = 8.46^{+0.42}_{-0.38}$ kpc, removing any tension with our estimate and that of the ESO group. We conclude that our estimate of $R_0 = 8.34 \pm 0.16$ kpc is consistent with that from the Galactic center stellar orbits and is likely the most accurate to date.

5.4. The Circular Rotation Speed at the Sun: Θ_0

Over the last four decades there have been many estimates of Θ_0 ranging from ∼170 → 270 km s^{-1} (Kerr & Lynden-Bell 1986; Olling & Merrifield 1998). Focusing the discussion to the more direct measurements, two recent studies favor a lower and one a higher value of Θ_0 than our estimate of $\Theta_0 = 240 \pm 8$ km s^{-1}. Koposov et al. (2010) model the orbit of the GD-1 stream from a tidally disrupted stellar cluster in the Milky Way halo and estimate $\Theta_0 + V_\odot = 221 \pm 18$, where the Dehnen & Binney (1998) solar motion component of $V_\odot = 5$ km s^{-1} was adopted. Recently, Bovy et al. (2012) modeled line-of-sight velocities of 3365 stars from APOGEE and find $\Theta_0 = 218 \pm 6$ km s^{-1}, but with a large value for the solar motion component in the direction of Galactic rotation, $V_\odot = 26 \pm 3$ km s^{-1}. Their full tangential speed $\Theta_0 + V_\odot = 242^{+10}_{-3}$ is consistent with our value of 252.2 ± 4.8 km s^{-1}, suggesting the discrepancy between the Bovy et al. and our results are probably caused by differences in the solar motion. However, another recent study by Carlin et al. (2012), modeling the Sagittarius tidal stream, yields Θ_0 estimates from 232 → 264 km s^{-1}.

Our data also strongly constrain the angular rotation of the Sun about the Galactic center, $(\Theta_0 + V_\odot)/R_0 = 30.57 \pm 0.43$ km s^{-1} kpc^{-1}. This value can be compared with an independent and direct estimate based on the proper motion of Sgr A*, interpreted as the reflex motion from the Sun's Galactic orbit, of 30.24 ± 0.12 km s^{-1} kpc^{-1} (Reid & Brunthaler 2004). For $R_0 = 8.34 \pm 0.16$ kpc, the proper motion of Sgr A* translates to $\Theta_0 + V_\odot = 252.2 \pm 4.8$ km s^{-1}, in good agreement with the parallax results. We conclude that Θ_0 exceeds the IAU recommended value of 220 km s^{-1} with >95% probability provided that $V_\odot \lesssim 23$ km s^{-1}. Clearly, independent *global* measures of $V_\odot$ are critical to establish Θ_0 and $\overline{V_s}$ with high accuracy.

Changing the value of Θ_0 would have widespread impact in astrophysics. For example, increasing Θ_0 by 20 km s^{-1} with respect to the IAU recommended value of 220 km s^{-1} reduces kinematic distances by about 10%, leading to a decrease of 20% in estimated young star luminosities, a corresponding decrease in estimated cloud masses, and a change in young stellar object ages. Estimates of the total mass of the dark matter halo of the Milky Way scale as $V^2_{\rm max} R_{\rm Vir}$. Since the maximum in the rotation curve ($V_{\rm max}$) and the Virial radius ($R_{\rm Vir}$) scale linearly with Θ_0, the mass of the halo scales as Θ^3_0, leading to a 30% increase in the estimate of the Milky Way's (dark-matter dominated) mass. This, in turn, affects the expected dark-matter annihilation signal (Finkbeiner et al. 2009), increases the "missing satellite" problem (Wang et al. 2012), and increases the likelihood that the Magellanic Clouds are bound to the Milky Way (Shattow & Loeb 2009).

5.5. The Hulse–Taylor Binary Pulsar and Gravitation Radiation

An interesting example of the effects of Galactic parameters on fundamental physics comes from the Hulse–Taylor binary pulsar. The dominant uncertainty in measuring the gravitational radiation damping of the binary's orbit comes from the need to correct for the effects of the Galactic accelerations of the Sun and the binary (Damour & Taylor 1991; Weisberg et al. 2010). These accelerations contribute ≈1% to the *apparent* orbital period decay. In 1993 when the Nobel Prize was awarded in part for this work, the IAU recommended values were $R_0 = 8.5 \pm 1.1$ kpc and $\Theta_0 = 220 \pm 20$ km s^{-1} (Kerr & Lynden-Bell 1986). Using these Galactic parameters, the formalism of Damour & Taylor, improved pulsar timing data of Weisberg, Nice, & Taylor, and a pulsar distance of 9.9 kpc, the binary's orbital period decays at a rate of 0.9994 ± 0.0023 times

that prediction from general relativity (GR). Using the improved Galactic parameters from the A5 fit ($R_0 = 8.34 \pm 0.16$ kpc and $\Theta_0 = 240 \pm 8$ km s^{-1}), gives a GR test value of 0.9976 ± 0.0008. This provides a three-fold improvement in accuracy. Both of these examples assumed a distance to the binary pulsar of 9.9 kpc (Weisberg et al. 2008). Given the improvement in the Galactic parameter values, the dominant uncertainty in the GR test now is the uncertain pulsar distance. A pulsar distance of 7.2 kpc would bring the GR test value to 1.0000 and a trigonometric parallax accurate to ±8%, which is possible with in-beam calibration with the VLBA, would bring the contribution of distance uncertainty down to that of the current Galactic parameter uncertainty. Alternatively, if one assumes GR is correct, the current improvement in Galactic parameters suggests that the Hulse–Taylor binary pulsar's distance is 7.2 ± 0.5 kpc.

This work was partially funded by the ERC Advanced Investigator Grant GLOSTAR (247078). The work was supported in part by the National Science Foundation of China (under grants 10921063, 11073046, 11073054 and 11133008) and the Key Laboratory for Radio Astronomy, Chinese Academy of Sciences. A.B. acknowledges support by the National Science Centre Poland through grant 2011/03/B/ST9/00627.

Facilities: VLBA, VERA, EVN

REFERENCES

Ando, K., Nagayama, T., Omodaka, T., et al. 2011, PASJ, 63, 45
Asaki, Y., Deguchi, S., Imai, H., et al. 2010, ApJ, 721, 267
Bartkiewicz, A., Brunthaler, A., Szymczak, M., van Langevelde, H. J., & Reid, M. J. 2008, A&A, 490, 787
Benjamin, R. A. 2008, in ASP Conf. Ser. 387, Massive Star Formation: Observations Confront Theory, ed. H. Beuther, H. Linz, & Th. Henning (San Francisco, CA: ASP), 375
Benjamin, R. A., Churchwell, E., Babler, B. L., et al. 2005, ApJL, 630, L149
Blaauw, A. 1985, in IAU Symp. 106, The Milky Way Galaxy, ed. H. Van Woerden et al. (Dordrecht: Reidel), 335
Blitz, L., & Spergel, D. N. 1991, ApJ, 379, 631
Bobylev, V. V., & Bajkova, A. T. 2010, MNRAS, 408, 1788
Bovy, J., Hogg, D. W., & Rix, H.-W. 2009, ApJ, 704, 1704
Bovy, J., Prieto, C. A., Beers, T. C., et al. 2012, ApJ, 759, 131
Bovy, J., & Rix, H.-W. 2013, ApJ, 779, 115
Brand, J., & Blitz, L. 1993, A&A, 275, 67
Brunthaler, A., Reid, M. J., Menten, K. M., et al. 2009, ApJ, 693, 424 (Paper V)
Burkert, A., Genzel, R., Bouché, N., et al. 2010, ApJ, 725, 2324
Carlin, J. L., Majewski, S. R., Casetti-Dinescu, D. I., et al. 2012, ApJ, 744, 25
Chang, C.-K., Ko, C.-M., & Peng, T.-H. 2011, ApJ, 740, 34
Choi, Y. K., Hachisuka, K., Reid, M. J., et al. 2014, ApJ, submitted
Choi, Y. K., Hirota, T., Honma, M., et al. 2008, PASJ, 60, 1007
Clemens, D. P. 1985, ApJ, 295, 422
Coskunoglu, B., Ak, S., Bilir, S., et al. 2011, MNRAS, 412, 1237
Damour, T., & Taylor, J. H. 1991, ApJ, 366, 501
Dehnen, W., & Binney, J. J. 1998, MNRAS, 298, 387
Do, T., Martinez, G. D., Yelda, S., et al. 2013, ApJL, 779, L6
Eyer, L., Holl, B., Pourbaix, D., et al. 2013, CEAB, 37, 115
Feast, M., & Whitelock, P. 1997, MNRAS, 291, 683
Finkbeiner, D. P., Slatyer, T. R., Weiner, N., & Yavin, I. 2009, JCAP, 09, 037
Ghez, A. M., Salim, S., Weinberg, N. N., et al. 2008, ApJ, 689, 1044
Gillessen, S., Eisenhauer, F., Fritz, T. K., et al. 2009a, ApJL, 707, L114
Gillessen, S., Eisenhauer, F., Trippe, S., et al. 2009b, ApJ, 692, 1075
Hachisuka, K., Brunthaler, A., Menten, K. M., et al. 2006, ApJ, 645, 337
Hachisuka, K., Brunthaler, A., Menten, K. M., et al. 2009, ApJ, 696, 1981
Hachisuka, K., Choi, Y. K., Reid, M. J., et al. 2014, ApJ, submitted
Hammersley, P. L., Garzón, F., Mahoney, T. J., López-Corredoira, M., & Torres, M. A. P. 2000, MNRAS, 317, 45
Hirota, T., Ando, K., Bushimata, T., et al. 2008, PASJ, 60, 961
Honma, M., Bushimata, T., Choi, Y. K., et al. 2007, PASJ, 59, 889
Honma, M., Hirota, T., Kan-Ya, Y., et al. 2011, PASJ, 63, 17
Honma, M., Nagayama, T., Ando, K., et al. 2012, PASJ, 64, 136
Immer, K., Reid, M. J., Menten, K. M., Brunthaler, A., & Dame, T. M. 2013, A&A, 553, 117
Kennicutt, R. C., Jr. 1981, AJ, 86, 1847
Kent, S. M., Dame, T. M., & Fazio, G. 1991, ApJ, 378, 131
Kerr, F. J., & Lynden-Bell, D. 1986, MNRAS, 221, 1023
Kim, M. K., Hirota, T., Honma, M., et al. 2008, PASJ, 60, 991
Koposov, S. E., Rix, H.-W., & Hogg, D. W. 2010, ApJ, 712, 260
Kurayama, T., Nakagawa, A., Sawada-Satoh, S., et al. 2011, PASJ, 63, 513
Liszt, H. S., & Burton, W. B. 1980, ApJ, 236, 779
McMillan, P. J. 2011, MNRAS, 414, 2446
McMillan, P. J., & Binney, J. J. 2010, MNRAS, 402, 934
Menten, K. M., Reid, M. J., Forbrich, J., & Brunthaler, A. 2007, A&A, 474, 515
Moellenbrock, G. A., Claussen, M. J., & Goss, W. M. 2009, ApJ, 694, 192
Morris, M. R., Meyer, L., & Ghez, A. 2012, RAA, 12, 995
Moscadelli, L., Cesaroni, R., Rioja, M. J., Dodson, R., & Reid, M. J. 2011, A&A, 526, 66
Moscadelli, L., Reid, M. J., Menten, K. M., et al. 2009, ApJ, 693, 406
Nagayama, T., Omodaka, T., Nakagawa, A., et al. 2011, PASJ, 63, 23
Niinuma, K., Nagayama, T., Hirota, T., et al. 2011, PASJ, 63, 9
Oh, C. S., Kobayashi, H., Honma, M., et al. 2010, PASJ, 62, 101
Olling, R. P., & Merrifield, M. R. 1998, MNRAS, 297, 943
Persic, M., Salucci, P., & Stel, F. 1996, MNRAS, 281, 27
Porcel, C., Garzon, F., Jimenez-Vicente, J., & Battaner, E. 1998, A&A, 330, 136
Reid, M. J. 1993, ARA&A, 31, 345
Reid, M. J., & Brunthaler, A. 2004, ApJ, 616, 872
Reid, M. J., Menten, K. M., Brunthaler, A., et al. 2009a, ApJ, 693, 397
Reid, M. J., Menten, K. M., Zheng, X. W., et al. 2009b, ApJ, 700, 137
Reid, M. J., Menten, K. M., Zheng, X. W., Brunthaler, A., & Xu, Y. 2009c, ApJ, 705, 1548
Roberts, W. W., & Yuan, C. 1970, ApJ, 161, 877
Rygl, K. L. J., Brunthaler, A., Reid, M. J., et al. 2010, A&A, 511, 2
Rygl, K. L. J., Brunthaler, A., Sanna, A., et al. 2012, A&A, 539, 79
Sandstrom, K. M., Peek, J. E. G., Bower, G. C., Bolatto, A. D., & Plambeck, R. L. 2007, ApJ, 667, 1161
Sanna, A., Reid, M. J., Dame, T., et al. 2012, ApJ, 745, 82
Sanna, A., Reid, M. J., Menten, K. M., et al. 2014, ApJ, 781, 108
Sanna, A., Reid, M. J., Moscadelli, L., et al. 2009, ApJ, 706, 464
Sato, M., Hirota, T., Honma, M., et al. 2008, PASJ, 60, 975
Sato, M., Hirota, T., Reid, M., et al. 2010a, PASJ, 62, 287
Sato, M., Reid, M. J., Brunthaler, A., & Menten, K. M. 2010b, ApJ, 720, 1055
Sato, M., Wu, Y. W., Immer, K., et al. 2014, ApJ, submitted
Savchenko, S. S., & Reshetnikov, V. P. 2013, MNRAS, 436, 1074
Schoenrich, R., Binney, J., & Dehnen, W. 2010, MNRAS, 403, 1829
Shattow, G., & Loeb, A. 2009, MNRAS, 392, 21
Shiozaki, S., Imai, H., Tafoya, D., et al. 2011, PASJ, 63, 1219
Sivia, D., & Skilling, J. 2006, Data Analysis: A Bayesian Tutorial (2nd ed.; New York: Oxford Univ. Press), 168
Wang, J., Frenk, C. S., Navarro, J. F., Gao, L., & Sawala, T. 2012, MNRAS, 424, 2715
Weisberg, J. M., Nice, D. J., & Taylor, J. H. 2010, ApJ, 722, 1030
Weisberg, J. M., Stanimirović, S., Xilouris, K., et al. 2008, ApJ, 674, 286
Wu, Y. W., Sato, M., Reid, M. J., et al. 2014, A&A, submitted
Xin, X.-S., & Zheng, X.-W. 2013, RAA, 13, 849
Xu, Y., Li, J. J., Reid, M. J., et al. 2013, ApJ, 769, 15
Xu, Y., Moscadelli, L., Reid, M. J., et al. 2011, ApJ, 733, 25
Xu, Y., Reid, M. J., Menten, K. M., et al. 2009, ApJ, 693, 413
Xu, Y., Reid, M. J., Zheng, W. W., & Menten, K. M. 2006, Sci, 311, 54
Zhang, B., Moscadelli, L., Sato, M., et al. 2014, ApJ, 781, 89
Zhang, B., Reid, M. J., Menten, K. M., et al. 2013, ApJ, 775, 79
Zhang, B., Reid, M. J., Menten, K. M., & Zheng, X. W. 2012a, ApJ, 744, 23
Zhang, B., Reid, M. J., Menten, K. M., Zheng, X. W., & Brunthaler, A. 2012b, A&A, 544, 42
Zhang, B., Zheng, X. W., Reid, M. J., et al. 2009, ApJ, 693, 419